NAVAL POSTGRADUATE SCHOOL

MONTEREY, CALIFORNIA

THESIS

DYNAMIC RESPONSE AND FAILURE OF 3D PRINTED CYLINDRICAL STRUCTURES SUBJECTED TO IMPACT LOADING

by

Preston B. Gibbons

June 2023

Thesis Advisor: Young W. Kwon
Co-Advisor: Jarema M. Didoszak

THIS PAGE INTENTIONALLY LEFT BLANK

REPORT DOCUMENTATION PAGE	*Form Approved OMB No. 0704-0188*

1. AGENCY USE ONLY *(Leave blank)*	**2. REPORT DATE** June 2023	**3. REPORT TYPE AND DATES COVERED** Master's thesis

4. TITLE AND SUBTITLE DYNAMIC RESPONSE AND FAILURE OF 3D PRINTED CYLINDRICAL STRUCTURES SUBJECTED TO IMPACT LOADING	**5. FUNDING NUMBERS**
6. AUTHOR(S) Preston B. Gibbons	
7. PERFORMING ORGANIZATION NAME(S) AND ADDRESS(ES) Naval Postgraduate School Monterey, CA 93943-5000	**8. PERFORMING ORGANIZATION REPORT NUMBER**
9. SPONSORING / MONITORING AGENCY NAME(S) AND ADDRESS(ES) N/A	**10. SPONSORING / MONITORING AGENCY REPORT NUMBER**

11. SUPPLEMENTARY NOTES The views expressed in this thesis are those of the author and do not reflect the official policy or position of the Department of Defense or the U.S. Government.

12a. DISTRIBUTION / AVAILABILITY STATEMENT Approved for public release. Distribution is unlimited.	**12b. DISTRIBUTION CODE** A

13. ABSTRACT (maximum 200 words)

The dynamic response and failure of 3D printed concentric cylinders with a fluid-filled annulus subjected to impact loading was examined throughout the course of this research. The cylinders, which have an outside radius of 70 mm (2.76 in), inside radius of 50 mm (1.97 in), wall thickness of 1 mm (0.04 in) and length of 257 mm (10.12 in) were with strain gages to measure strain along the longitudinal and hoop directions when impacted with a pendulum. Three primary cases were investigated: air-filled annulus at ambient pressure, water filled annulus, and pressurized air-filled annulus. Within the primary cases, four subcases were also explored: 100% and 50% water-filled annulus, and an annulus pressurized to 2 and 4 psi. In each case, the cylinders were placed horizontally while being constrained at both ends and impacted with a pendulum at the center. Throughout the experimentation, the strain gage data and applied impact forces were collected and examined to better understand the effect of fluid structure interaction of a cylindrical structure. The data were compared to identify the effect of varied annulus conditions on both the inner and outer cylinder walls.

14. SUBJECT TERMS 3D printed, dynamic response, impact loading, strain response, 3D printed structures, 3D printed material science, fluid-structure interaction	**15. NUMBER OF PAGES** 65
	16. PRICE CODE

17. SECURITY CLASSIFICATION OF REPORT Unclassified	**18. SECURITY CLASSIFICATION OF THIS PAGE** Unclassified	**19. SECURITY CLASSIFICATION OF ABSTRACT** Unclassified	**20. LIMITATION OF ABSTRACT** UU

NSN 7540-01-280-5500

Standard Form 298 (Rev. 2-89)
Prescribed by ANSI Std. 239-18

THIS PAGE INTENTIONALLY LEFT BLANK

Approved for public release. Distribution is unlimited.

DYNAMIC RESPONSE AND FAILURE OF 3D PRINTED CYLINDRICAL STRUCTURES SUBJECTED TO IMPACT LOADING

Preston B. Gibbons
Ensign, United States Navy
BSCE, University of Memphis, 2022

Submitted in partial fulfillment of the
requirements for the degree of

MASTER OF SCIENCE IN MECHANICAL ENGINEERING

from the

NAVAL POSTGRADUATE SCHOOL
June 2023

Approved by: Young W. Kwon
Advisor

Jarema M. Didoszak
Co-Advisor

Brian S. Bingham
Chair, Department of Mechanical and Aerospace Engineering

THIS PAGE INTENTIONALLY LEFT BLANK

ABSTRACT

The dynamic response and failure of 3D printed concentric cylinders with a fluid-filled annulus subjected to impact loading was examined throughout the course of this research. The cylinders, which have an outside radius of 70 mm (2.76 in), inside radius of 50 mm (1.97 in), wall thickness of 1 mm (0.04 in) and length of 257 mm (10.12 in) were with strain gages to measure strain along the longitudinal and hoop directions when impacted with a pendulum. Three primary cases were investigated: air-filled annulus at ambient pressure, water filled annulus, and pressurized air-filled annulus. Within the primary cases, four subcases were also explored: 100% and 50% water-filled annulus, and an annulus pressurized to 2 and 4 psi. In each case, the cylinders were placed horizontally while being constrained at both ends and impacted with a pendulum at the center. Throughout the experimentation, the strain gage data and applied impact forces were collected and examined to better understand the effect of fluid structure interaction of a cylindrical structure. The data were compared to identify the effect of varied annulus conditions on both the inner and outer cylinder walls.

THIS PAGE INTENTIONALLY LEFT BLANK

TABLE OF CONTENTS

THIS PAGE INTENTIONALLY LEFT BLANK

LIST OF FIGURES

LIST OF TABLES

THIS PAGE INTENTIONALLY LEFT BLANK

ACKNOWLEDGMENTS

I would like to thank my advisor, Dr. Young Kwon; co-advisor, Dr. Jarema Didoszak; and colleague, Michael O'Donell, for their guidance, wisdom, and support throughout the research process.

THIS PAGE INTENTIONALLY LEFT BLANK

I. INTRODUCTION

A. BACKGROUND

Cylindrical structures are commonly utilized within all forms of industry such as aeronautical, maritime, energy, and public utility. Oftentimes, these structures are used as structural members or as a means of conveyance of material. Regardless of their use, most cylindrical structures are subjected to the effects of fluid-structure interaction (FSI). FSI can occur internally, such as the case of pipe flow, externally, such as wind or water, or internally and externally, such as an underwater pressure hull. Within FSI, there are two groups of study. The first is aptly named the flow or vortex induced problem. This occurs as a fluid flows within or around a structure, leading to oscillations or vibrations within the structure itself [1]. One example of this is the swaying and oscillation that occurs in skyscrapers due to the interaction of wind at the structure's interface which generates vortices. This problem is of great significance and an extensive amount of research has been dedicated toward improving the design and response of these buildings, such as by using a tuned mass damper, to mitigate the effects of this FSI problem [2]. The second variety of FSI problems are those in which the fluid is excited via a solid body. This occurs when a structure containing a fluid mechanically interacts with the fluid. Such instances occur within liquid tanks during seismic activity or in the event of an impact of a fluid-containing structure [3]. The problem involving the impact of a fluid filled structure is of significant interest due to the utility and applicability of the problem to industry.

B. STATE OF THE ART

The FSI of impact loaded structures has been studied extensively. Commonly, metallic structures interfaced with water are studied to optimize current models and structure design [4]. Recently, researchers have examined the dynamic response of metallic pipes containing water at various flow conditions while subjected to impact loading [5]. This research found that the flow conditions significantly altered the strain and frequency response of the pipe. Building upon that, researchers began examining the response of fluid-coupled concentric cylinders made from composites [6–8]. This research involved

two independent composite structures with water within the annulus which was then subjected to a low-velocity impact force. The water level and impact force were varied to analyze the behavior of the internal fluid and its effect on the internal structure. While considerable research has been conducted on the FSI of impact loading of metallic and composite structures, the strength of these materials is greater than the forces generated by the low velocity impacts. Data and research are not available for understanding the effects of the annulus conditions on fluid-coupled structures during failure. Thus, this research aims to fill the gaps in the understanding of how failure of the structure and varied fluid-coupling methods affects the strain and force response of a cylindrical structure.

C. OBJECTIVES

This study's objective is to investigate dynamic responses and failure of cylindrical structures resulting from mechanical impact loading as the structures are subjected to various kinds of FSI. The control case had just atmospheric air in the annulus while other cases had water or pressurized air in the annulus. The water level was either 50% or 100% in the annuli, and the air pressure was either 13.8 kPa (2 psi) or 27.6 kPa (4 psi). All the test structures were fabricated using a 3D printer with PLA material. Every test structure was made of two concentric cylinders with a uniform spacing of their annulus. A force sensor and strain gages were used to monitor dynamic responses and failure of the test cylinders.

II. EXPERIMENTAL SETUP

This chapter will discuss the methodology for the research conducted within this paper, including but not limited to the design of components used, printing processes and parameters, specimen preparation, and experimental design.

A. COMPONENT DESIGN

Four individual components were drafted and printed to conduct the experimentation for research; namely one sealing cap, two mounting brackets, and one cylinder. Each of the components were designed in the computer-aided design (CAD) software SolidWorks 2022.

1. Cylinder Design

The cylinders, used as test specimen within the research, consist of two concentric cylinders with an inner radius of 51 mm (2.01 in.), outer radius of 71 mm (2.80 in.), height of 257 mm (10.12 in.), and outside wall thickness of 1 mm (0.04 in.). The base of the cylinder was enclosed with 3D printed material with a thickness of 3 mm (0.12 in.) to minimize the possibility of leaks throughout experimentation while the top was left unsealed. Figures 1 and 2 depict the design and dimensions of the cylinders to be used throughout the research.

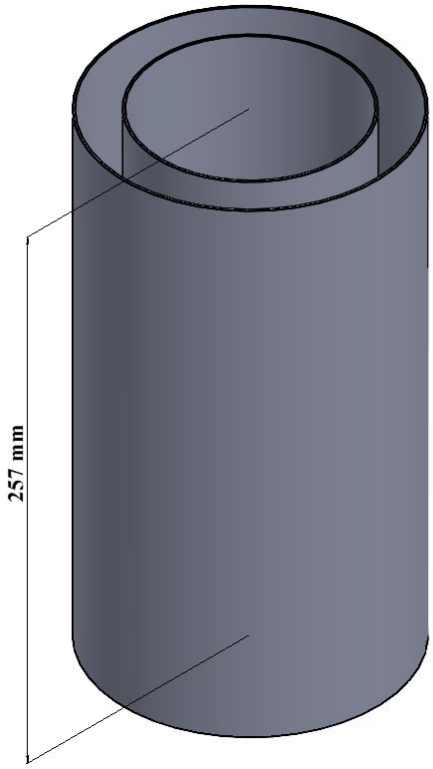

Figure 1. CAD Model of Cylinder Height

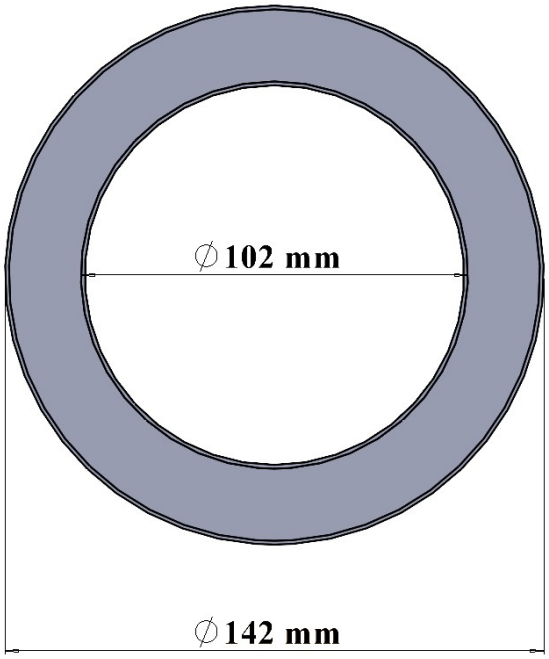

Figure 2. Top View of Inner and Outer Radii of Cylinder

2. Cap Design

A cap was designed for two purposes: providing an air and watertight seal within the annulus of the cylinder and permitting access for the introduction of water and pressurized air once the cylinder is sealed. The cap design was kept simple for ease of production. The design consisted of a 2 mm (0.08 in.) thick disk with concentric shoulders with a wall thickness of 1 mm (0.04 in.), outer radius of 71.75 mm (2.82 in.) and inner radius of 49.95 mm (1.97 in.). The shoulders were designed so that they would extend 10 mm (0.39 in.) beyond the outer wall of the concentric cylinders of the test specimen. To provide access to the annulus of the cylinder once sealed, a 14.63 x 14.63 x 8 mm (0.58 x 0.58 x 0.31 in.) valve block with a pilot hole of radius 4 mm (0.16 in.) was placed atop the cap so that a Schrader valve could be affixed and sealed, permitting the introduction of air and water to the annulus. Preceding production of the cap, the valve block was drilled and tapped to accept the threads of a 1/8 in. NPT (National Pipe Thread) brass Schrader valve. Figures 3–5 illustrate the final cap design used throughout the experimentation trials.

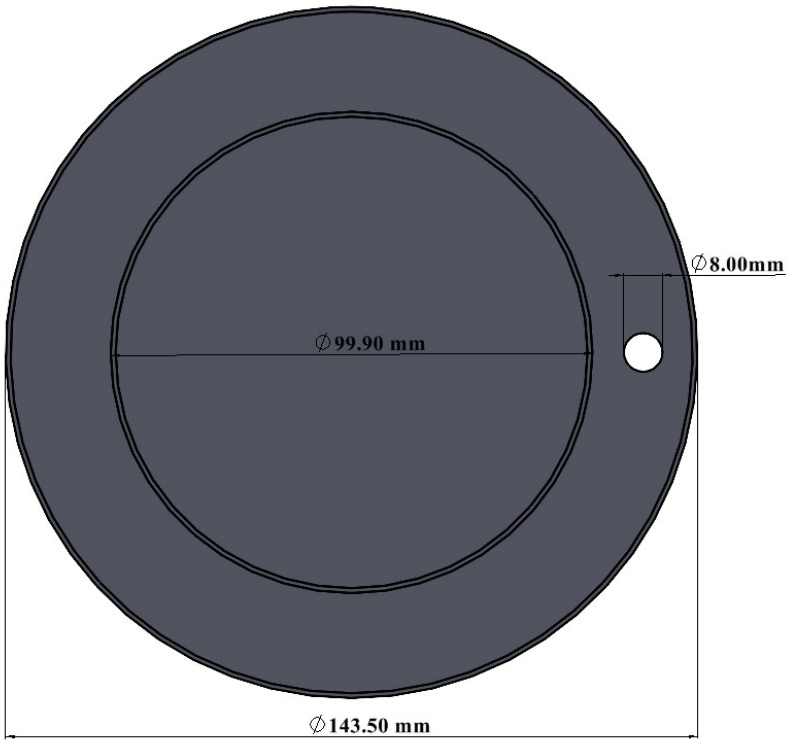

Figure 3. Bottom View of Cap Design

Figure 4. Side View of Cap Design

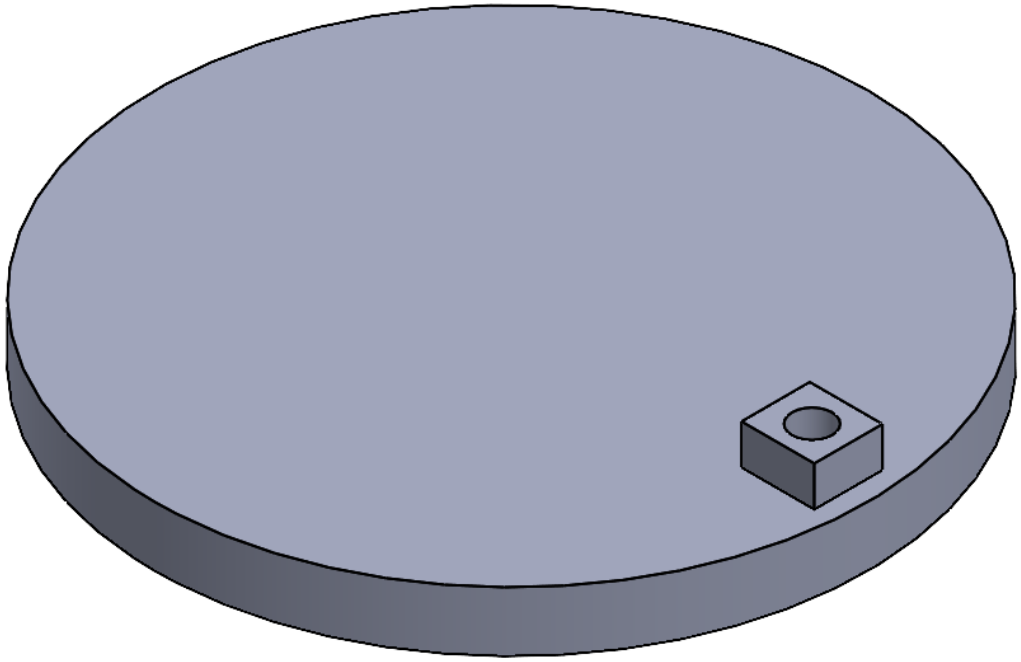

Figure 5. Isometric View of Cap Design

3. Mount Designs

Two mounts were created to rigidly support the cylinder at both ends during experimentation trials. Two separate designs were required for proper fitment around the circumference of the test specimens, one design for the capped end and the other for the sealed end. The mounts were identical in all aspects aside from a 0.75 mm (0.03 in.) inlay placed within the inside diameter of the mount to allow the cap to be fitted on the cylinder and placed tightly within the mount. The mounts were designed with a thickness of 25 mm

(0.98 in) to maximize the unsupported length of the cylinder, minimizing any effects the mounts may impose on the results. To mitigate impact energy losses, the mounts were designed with through-holes at the base of the mount that were drilled and fitted with bolts and affixed to a rigid mounting plate. Figures 6 through 8 show the mount designs used within the experiments conducted.

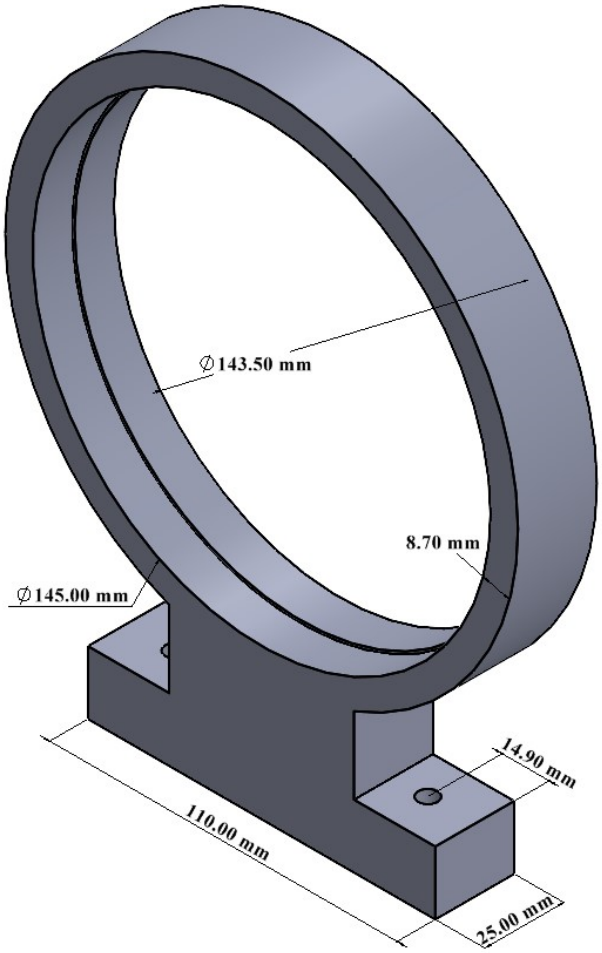

Figure 6. Isometric View of Mount for Capped Side

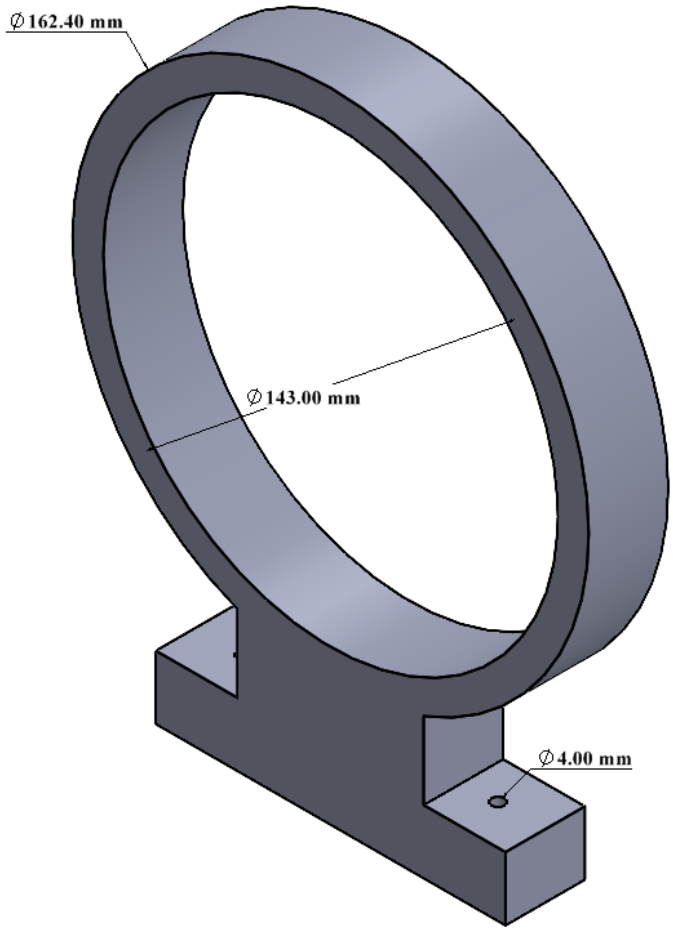

Figure 7. Isometric View of Mount for Sealed Side

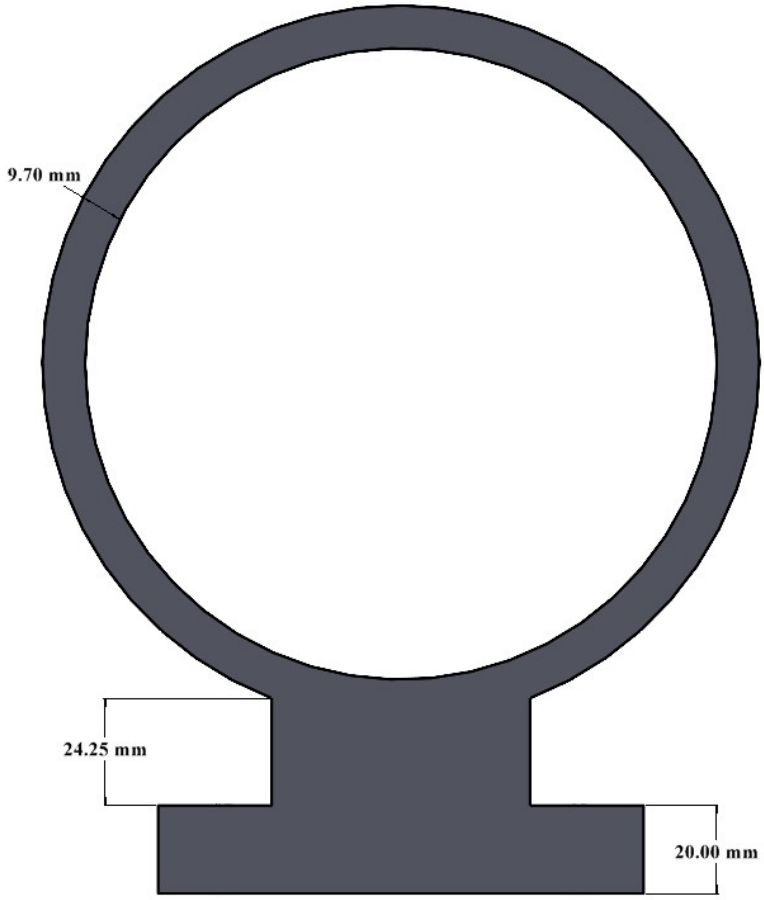

Figure 8. Front View of Mount

B. PRINTING PROCESS/PARAMETERS

The printer used throughout the entirety of the research was the commercially available UltiMaker S5 Pro Bundle that features a fully enclosed build volume of 330 x 240 x 300 mm (13.0 x 9.45 x 11.81 in.), six bay material station, and dual extrusion nozzles [9]. The component designs were converted to STL files and parameterized using Ultimaker Cura Slicer, a software that allows the user to specify and optimize the parameters desired for a specific print.

Within 3D printing, the print parameters selected for component production are nearly as important as the design itself. For this reason, print parameters were carefully chosen through a series of test prints in which the following criteria were qualitatively

analyzed: bed adhesion, layer adhesion, susceptibility to warping of the final part, and uniform layer deposition. For optimization of these criteria, it was found that layer height, print temperature, build plate temperature, and print speed were the settings that significantly altered the outcome of the component. Thus, these parameters were iteratively adjusted to achieve a quality part that would be reproducible for production of multiple samples. The parameters of each respective component are tabulated in Table 1.

Table 1. Print Parameters of Components

Component	***Material***	***Layer Height (mm)***	***Infill Density (%)***	***Print Temp. (°C)***	***Build Plate Temp. (°C)***	***Print Speed (mm/s)***
Cylinder	Polylactic Acid (PLA)	0.15	100	200	60	70
Cap	Polylactic Acid (PLA)	0.15	100	200	60	70
Mounts	Polycarbonate	0.15	45*	285	125	50

*Gyroid infill pattern used to maximize rigidity in all dimensions.

While the research was aimed towards understanding the mechanics of impact loading of different annuli conditions of concentric PLA cylinders, polycarbonate was used for mounts for its superior properties to PLA in regard to tensile strength. Depending upon the orientation the part is printed at and relative angle of subsequent layers, polycarbonate has a maximum tensile strength of approximately 50 MPa, compared to PLA's tensile strength of 45 MPa [10]. By printing the mounts in polycarbonate, the infill density could be significantly reduced, as seen in Table 1, effectively using less material and time to complete prints with similar component performance.

C. EXPERIMENT DESIGN

As aforementioned, the purpose of the research conducted is to develop an understanding of the interaction between cylindrical walls and a fluid filled annulus at various conditions when subjected to an impact load causing failure. The design of the experiment aimed to accomplish this by investigating the impact response of the cylinders

during three primary cases and four sub-cases from a weighted pendulum dropped from an angle of 45°, as measured from the vertical axis. The pendulum setup up is shown in Figure 9.

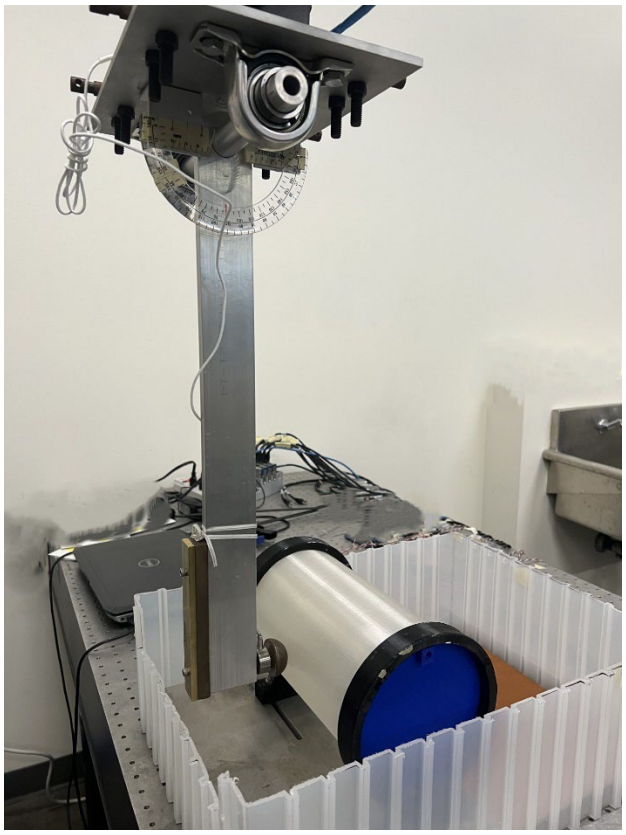

Figure 9. Pendulum and Cylinder Setup

The primary cases consisted of a control with the annulus filled with air at ambient pressure, the annulus filled with water, and the annulus pressurized. Two sub-cases were explored for each of the primary cases involving other than ambient annulus conditions. The sub-cases for the water filled annulus involved filling the annulus to 50% and 100% by volume. The pressurized annulus was tested at 13.8 kPa (2 psi) and 27.6 kPa (4 psi). To ensure repeatability and the integrity of results, each case was conducted at least two times. Table 2 consolidates the design of the experimental trials.

Table 2. Experimental Design Conditions

Sample Type	***Annulus Condition***
Control	Ambient pressure
Water filled	100% water filled
	50% water filled
Pressurized	27.6 kPa
	13.8 kPa

Motivation for choosing a drop angle of 45° was based on a series of preliminary trials. The research conducted aimed to investigate the impact response prior to and at failure, which required the impact force to be sufficient to induce failure of the material after multiple impacts, but not great enough to cause failure on the first impact. The effects of impacts from 30°, 45°, 60°, 75°, and 85° pendulum drop angles were explored. Within the preliminary trials conducted, all angles aside from 45° and 30° resulted in the failure of at least one cylinder from each annulus case, defined as interlayer cracks or shattering of the outside cylinder's wall, after one impact from the pendulum. The 30° angle was not chosen as a matter of efficiency as the number of blows until failure were too great for timely data processing.

D. MEASUREMENT EQUIPMENT

Throughout experimentation, a load cell and strain gages were used for collection of data of the impact event. The load cell was placed at the end of the pendulum and attached to a semi-spherical steel impactor and measured the impact force of the pendulum strike. Measuring the strain-response of the cylinders were eight linear strain gages, illustrated in Figure 10.

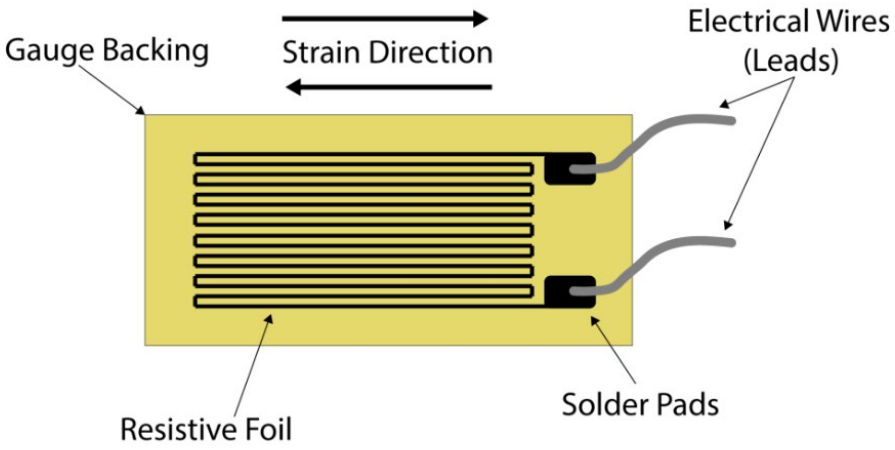

Figure 10. Strain Gage Source: [11]

Fundamentally, the strain gage is a Wheatstone bridge, a device commonly used to measure resistance, that is rigidly attached to a base material. As deformation, or strain, occurs within the base material, it is transferred to the strain gages. This results in a change of resistance within the gage, which can be directly correlated to strain by a value known as the gage factor. For all tests performed within this research all strain gages had an initial resistance of 350 Ohms, gage factor of 2.13, and tolerance of 0.30%.

Four points of interest were studied throughout experimentation, shown in Figure 11. The longitudinal and hoop strain were gathered from the outside face of the outer cylinder and inside face of the inner cylinder. The strain gages on each cylinder were placed at points approximately 180° away from one another. The nomenclature used throughout experimentation is also depicted in the Figure 11. Strain gages attached to the outer cylinder were called front or back, or "F" and "B," and strain gages placed on the inner cylinder were called inner front or inner back, "iF" and "iB," depending upon their position relative to the impact point.

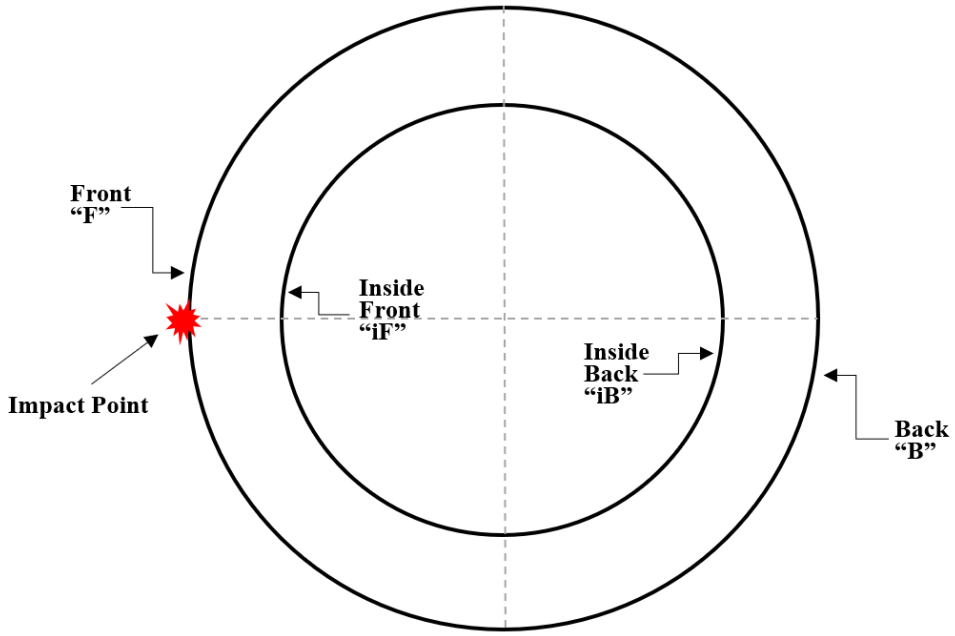

Figure 11. Strain Gage Locations

Since each individual strain gage measures strain in one dimension, two strain gages were attached to the sample perpendicular to one another at each point of interest. Dependent upon the direction of the strain to be measured, the strain gages were assigned a surname of "X" for longitudinal and "Y" for hoop strain. For the most accurate results of the material's strain response from the impact, the strain gages located on the front of the sample were placed as close to the point of impact as possible, taking caution to not allow for the semi-spherical impactor to contact the strain gages at any point during testing. Figure 12 shows the orientation of the strain gages on the front of the sample, which was repeated at every point of interest.

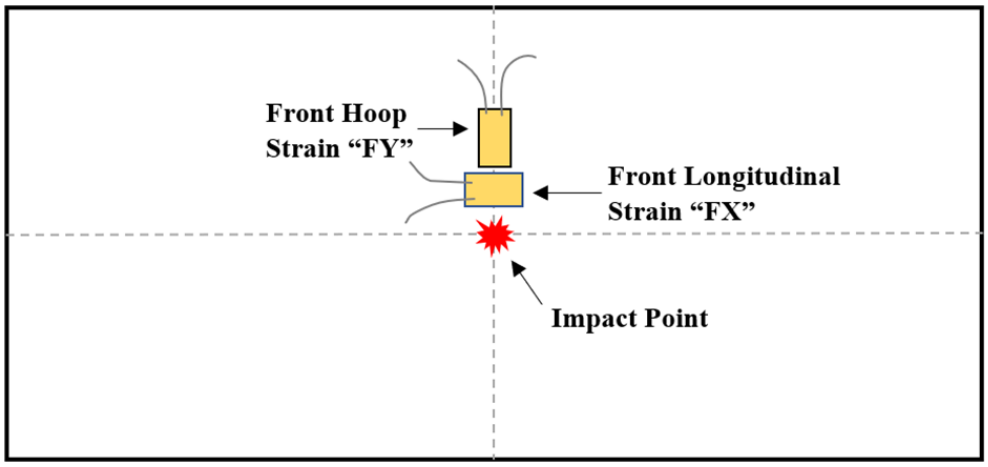

Figure 12. Front View of Cylinder with Strain Gage Orientation

E. SAMPLE PREPARATION

Prior to testing, it was important that the samples were adequately prepared for accurate and repeatable results. Prior to affixing the strain gages, the area in which they were to be placed was sanded with 400 grit sandpaper. This step ensured better contact and adhesion of the strain gages and epoxy resin used. Next, the area was wiped with acetone, allowed to dry, then further wiped with methanol. The strain gages were then taped to the cylinder at the desired location. An epoxy, Micro-Measurements M-Bond AE-10, was mixed according to the included instructions. A drop of epoxy was placed under each of the strain gages and then the strain gages were taped back down to the cylinder. Force was applied along the longitudinal axis of each strain gage to ensure complete coverage of the epoxy under each strain gage. The samples were then set aside to allow to cure for 24 hours. Upon completion of curing the strain gage wires were attached, with the positive wire attached to one strain gage lead, and the ground and neutral attached to the other strain gage lead. To ensure continuity of the circuit, a voltmeter in the Ohms measurement setting was used to check for a resistance of 350 Ohms. Once continuity of the circuit for each strain gage was ensured, the cylinder was placed in the mount and bolted to the aluminum mounting plate.

The procedure was followed for each sample; however, additional steps were required for the samples with water and pressurized air in the annulus. For these cases, a marine sealant was applied to the underside and outer edges of the cap. This ensured a water and airtight seal to prevent any leakage throughout testing. For the case where a water filled annulus was being investigated, the pilot hole printed in the cap was sealed using the marine sealant. In the pressurized annulus case, a Schrader valve, sealed with Teflon sealing tape, was screwed into the cap.

The strain gages and force sensor were wired to modules that were placed in a chassis produced by National Instruments. The software used for collection of all data was LabVIEW which collected and recorded the magnitude of impact force and strain as measured by the sensors.

F. TESTING PROCEDURE

Following preparation, the sample was placed in the mount and bolted to an aluminum mounting plate as shown in Figure 13.

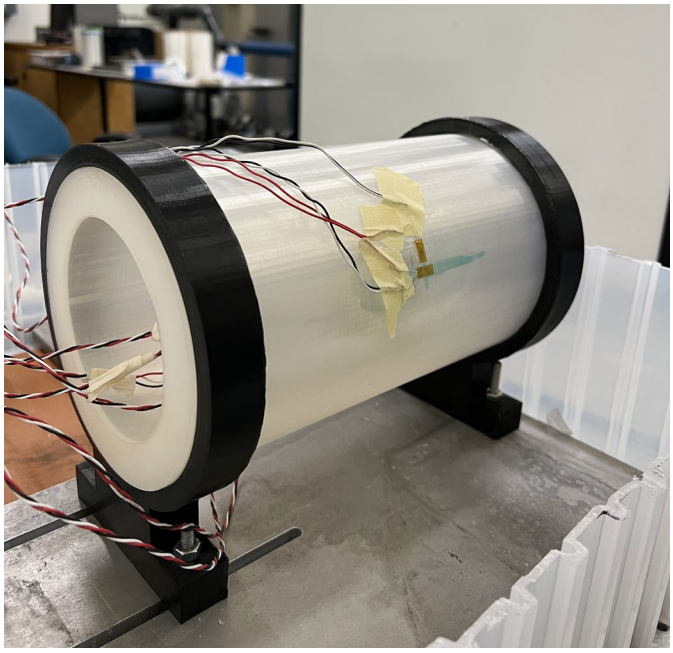

Figure 13. Cylinder Test Setup

The cylinder was placed in the mount so that the impactor would make contact at the center point 90° from the top and 127 mm (5 in) from the sides, shown in Figure 14.

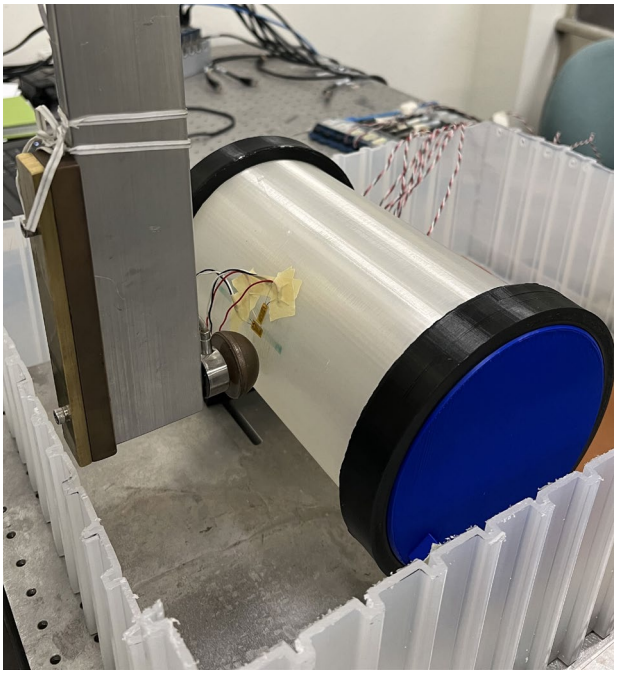

Figure 14. Test Setup with Pendulum

Once in place, the strain gages were calibrated within the LabVIEW software. The pendulum arm was raised to 45° and dropped in free-fall. Once contact was made with the cylinder, the pendulum arm was caught, to not allow for any additional contact, and the force and strain data for the blow was recorded. The trials were completed until the cylinder failed, after which the number of blows until failure was also recorded. Throughout the research, failure was defined by any breach, such as cracking or shattering of the walls of the cylinder.

THIS PAGE INTENTIONALLY LEFT BLANK

III. RESULTS AND DISCUSSION

Within this chapter, the results gathered from the strain and force gages are presented and discussed. From this data, determinations of the dynamic behavior of each annulus condition will be produced.

A. NUMBER OF BLOWS

As mentioned in the previous chapter, each annulus case was tested at least two times to ensure consistency. However, throughout experimentation, some of the annulus cases produced inconsistent results. Thus, it was necessary to test some annulus cases numerous times. Table 3 provides the number of blows each sample of an annulus case withstood until failure.

Table 3. Number of Blows Until Failure

Annulus Condition	Control				50% Water				100% Water		13.8 kPa		27.6 kPa	
Number of Blow Until Failure	25	6*	1	83*	37†	41†	1	46	1	1	2	1	2	5

*Samples affected by delamination.

†Samples affected by sample preparation.

In the case of the control and 50% water cases, four trials were conducted to achieve results that were consistent in the number of blows until failure. The inconsistency within the results was found to be caused by inconsistency in the production of the samples and sample preparation. The manufacture of parts through 3D printing is affected by ambient conditions of the environment in which they are produced, and upon closer inspection of the failed samples, it was discovered that delamination of the two layers that the outer cylinder walls were comprised of had occurred prior to testing. This was inferred to have been caused by the varying ambient conditions, such as temperature and humidity, within the print chamber. To mitigate further instances of this issue impacting results, each

completed print sample was visually inspected for delamination and rejected if found to be present. In the case of the 50% water filled cases, it was found that the caps were not adequately sealed prior to testing; thus, a complete seal of all subsequent samples was ensured prior to testing. Despite the wide range in the number of blows until failure in the control and 50% water filled cases, it was determined through further analysis of the results that, on average, the samples behaved in a consistent manner when subjected to an impact load and thus sufficient for use in this research.

As seen by the number of blows until failure, on average, the control and 50% water filled case are distinctly different than those of the other annuli type. Thus, it was expected that the strain of the outer cylinders within these cases would be similar, which will be explored later in this paper.

B. FAILURE MODE

The failure mode remained consistent, with little deviation, across all samples. As expected, the failure occurred in the hoop direction, perpendicular to the longitudinal axis of the sample as tested, between the printed layers of the cylinder. This is the result of the interlayer strength and stiffness of 3D printed materials being significantly less than that of the pre-production filament [12]. The failure crack propagated roughly ¼ the circumference of the outer cylinder in each case tested.

The crack, denoted within the red rectangle and colored with blue ink in Figure 15, originated from the point of impact and propagated circumferentially around the outside cylinder. For some cases, as shown in Figure 15, the crack propagated through the FX strain gage, rendering the data from the last blow at that strain gage unusable

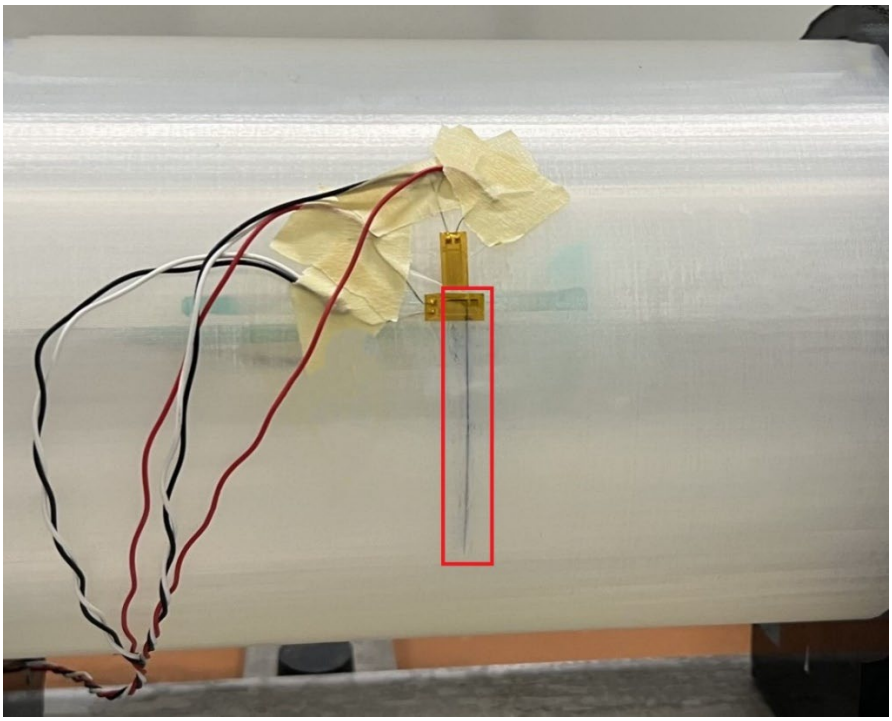

Figure 15. Failure Mode

C. FORCE DATA

1. Force of Impact Prior to Failure

It was speculated that the force of impact would vary as a function of annulus conditions as the fluid-filled annulus was expected to stiffen the cylinder wall or act behave in a manner that dampened the impact load. Figure 16 illustrates the average force-time history of each blow before failure.

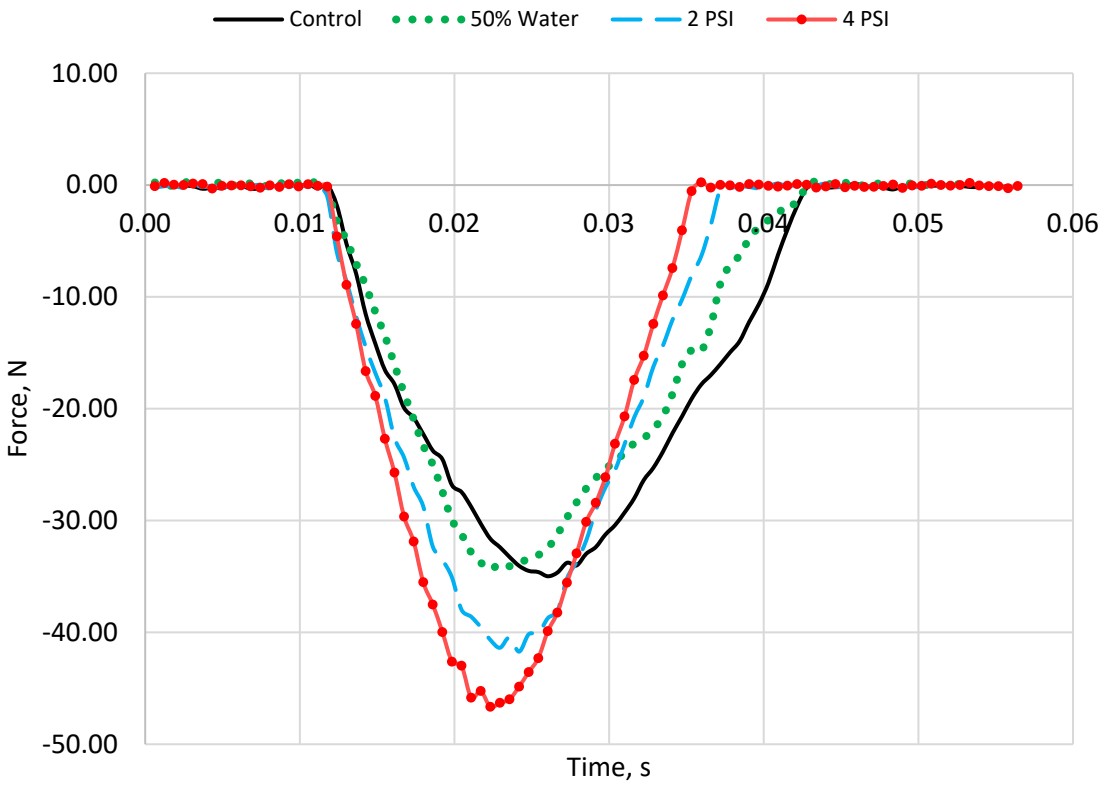

Figure 16. Average Force of Impact Prior to Failure

The average force of impact of each blow at each case before failure is shown in Figure 16, with the exception the 100% water filled annulus case. Data was not available for the 100% water filled case as each trial resulted in failure after one blow. The results show a clear trend among the various annulus conditions regarding impact force. The curves show that the pressurized annuli cases resulted in the largest impact forces and the 50% water case having the smallest impact force, with the control case slightly larger. The control and 50% water filled cases exhibit similar peak compressive force magnitudes at -35.2 N (7.91 lbf) and -34.4 N (7.73 lbf) respectively. This data aligns with and was expected when compared with the data found in Table 3. The average number of blows until failure across all trials was calculated to be 29 for the control case and 31 for the 50% water filled case, within the limits of reasonable error. While the magnitude of the forces between the control and 50% water filled cases are similar, the rate at which the force is applied and removed differs. The control case exhibits an observable decrease in the rate

at which force is applied at around -20 N (4.50 lbf). This is believed to have been caused by the greater deformation of the impact site of the control case as compared to that of the 50% water filled case; in which the water dissipated some of the impact force before further deformation occurred. Comparable results can be seen in the force-time histories of the 13.8 kPa (2 psi) and 27.6 kPa (4 psi) cases. The magnitude of peak force and rate of force applied for the 27.6 kPa (4 psi) case was greater than that of the 13.8 kPa (2 psi) with forces averaging -46.7 N (10.5 lbf) and -41.7 N (9.37 lbf) respectively. The force rate of the 27.6 kPa (4 psi) case is marginally higher due to the increased internal pressure within the annulus, resulting in less deformation of the sample, and subsequently a greater impact force.

2. Force of Impact at Failure

The force-time histories at the time of failure were graphed to examine if the annulus condition affected how force was applied at failure, shown in Figures 17 and 18.

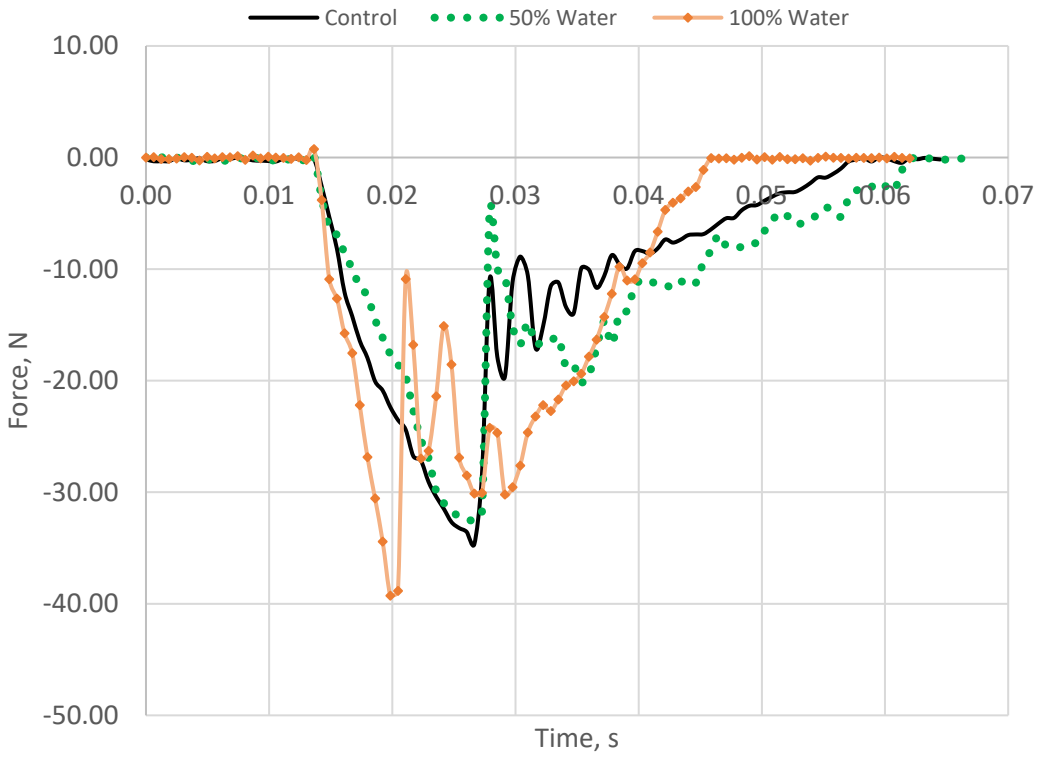

Figure 17. Force-Time Histories at Failure of Control and Water Cases

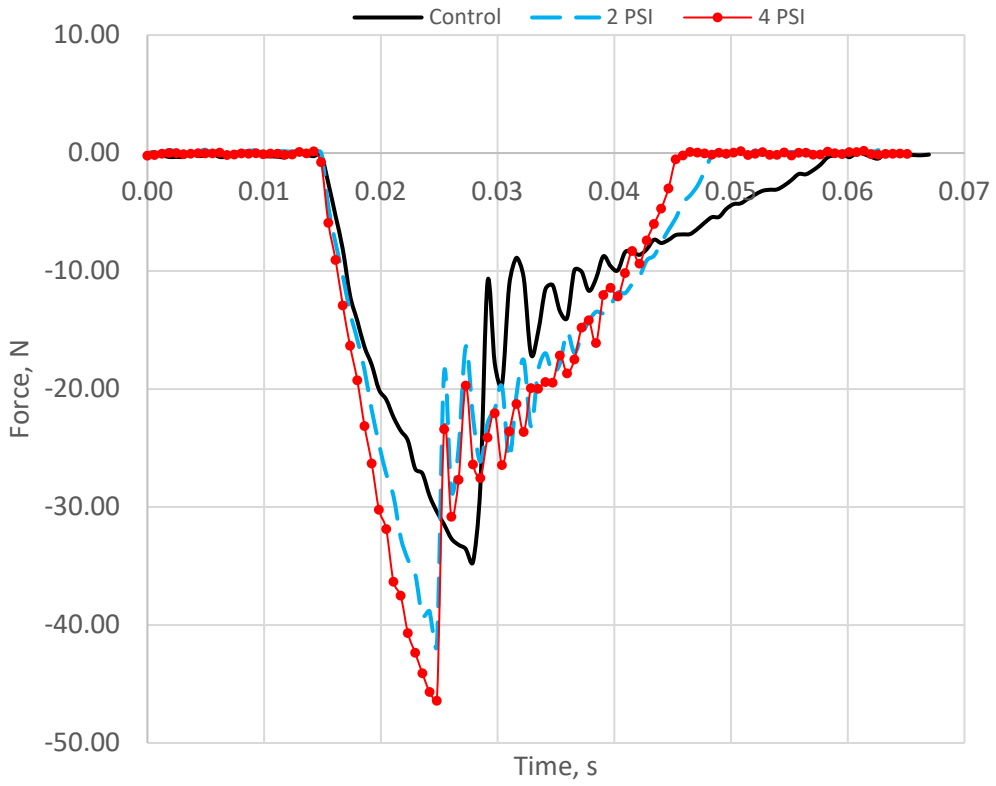

Figure 18. Force-Time Histories at Failure of Control and Pressurized Cases

Prior to failure, the graphs depicted half-sine curves with a gradual increase and decrease in force magnitude. However, when failure occurred, the impact force dropped sharply from its peak magnitude. The curves depicted in Figures 16 and 17 are similar to those found in Figure 15, regarding peak force and the rate at which force is applied. The consistency of each curve's shape in Figures 17 and 18 suggests the failure mode is the same, further validating the findings in this chapter.

3. Strain of Outer Cylinder Prior to Failure

Strains of the outer cylinder in response to the impact force were compared to further understand how the structure reacts at distinct locations across its circumference. The strains of the outer cylinder for each case are shown in Figures 19 through 22.

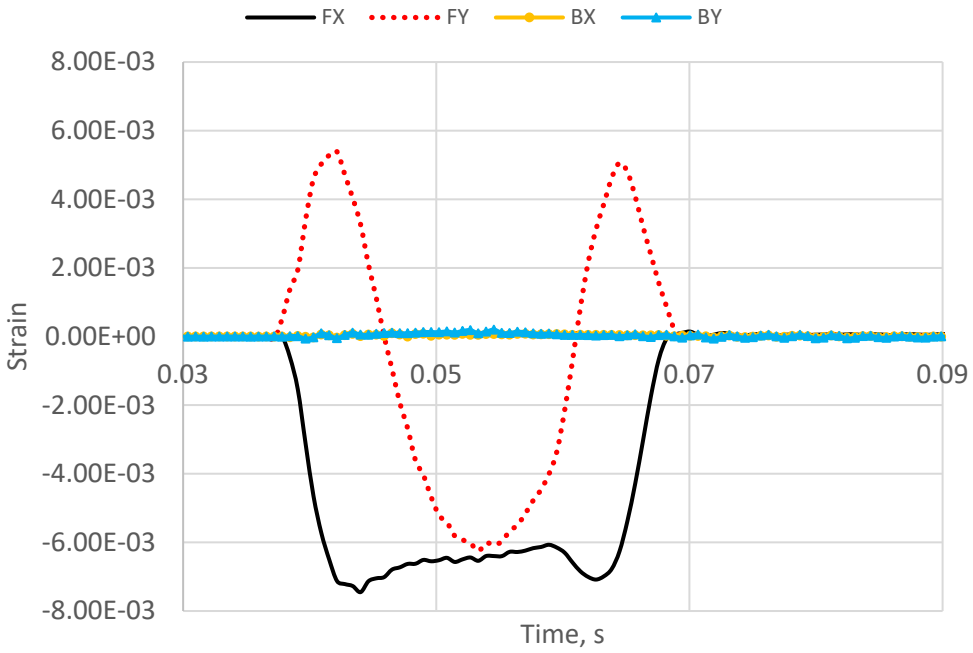

Figure 19. Outer Strain of Control

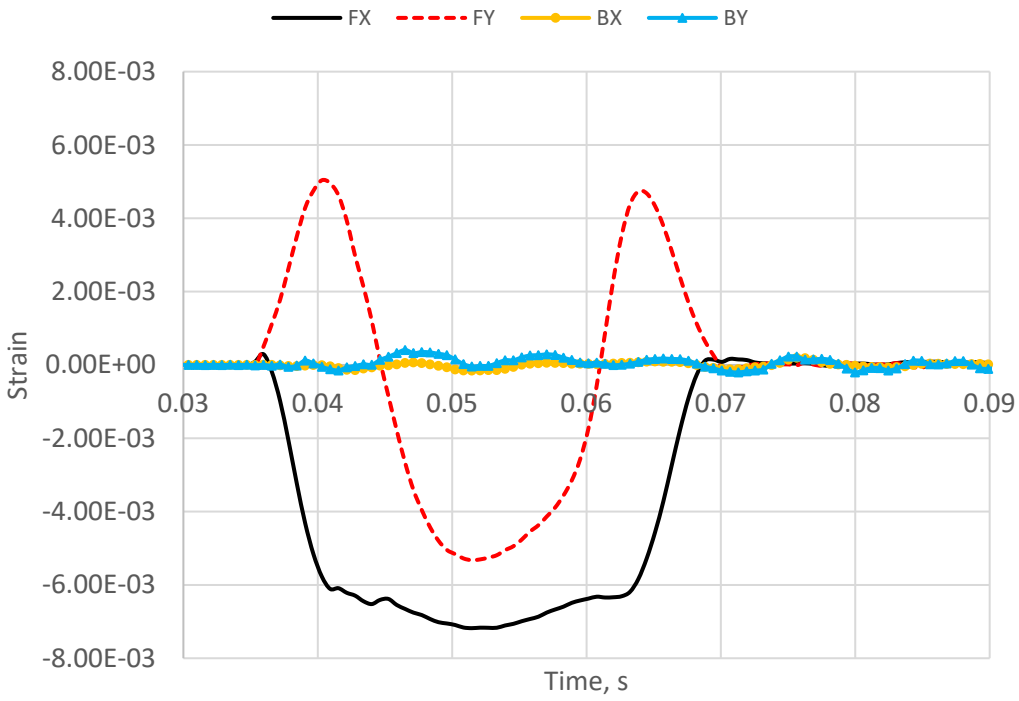

Figure 20. Outer Strain of 50% Water Filled

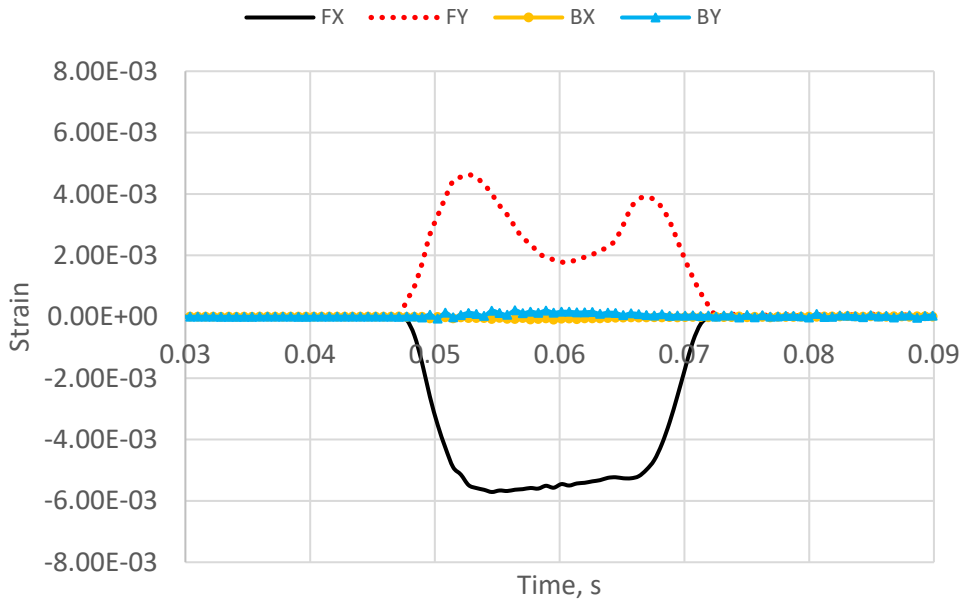

Figure 21. Outer Strain of 13.8 kPa

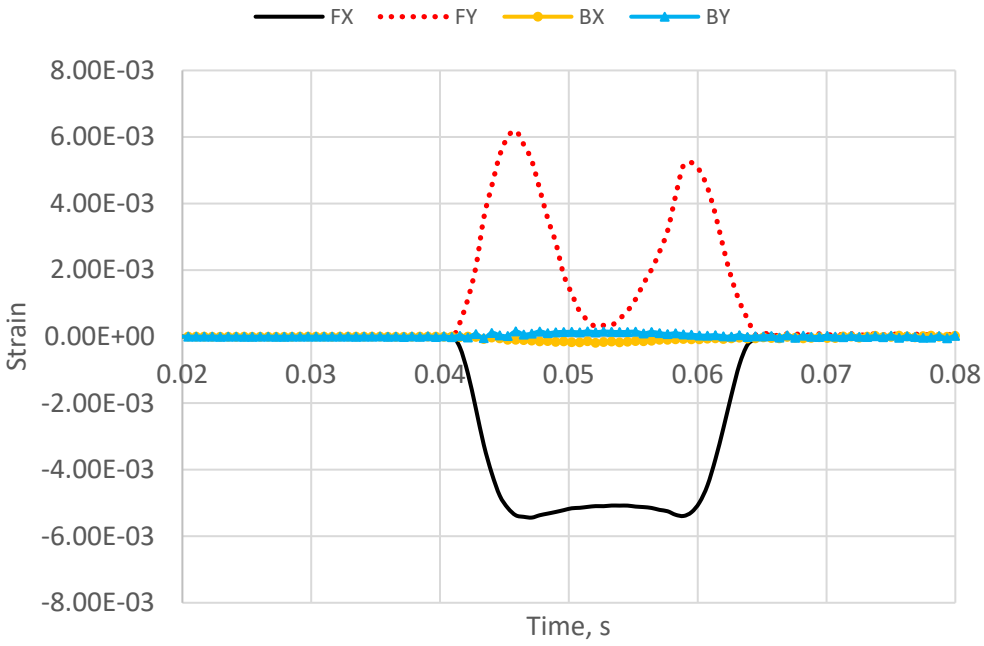

Figure 22. Outer Strain of 27.6 kPa

a. Front Longitudinal Strain "FX" Prior to Failure

In each of the strain time histories of the "FX" strain gage, data depicted a trapezoidal curve with peak strain values ranging from -7.45E-3 to -5.44E-3. The control case experienced the largest strain, closely followed by the 50% water filled case. These results were expected as they corroborate with the force-time histories of each of the cases, aside from the 50% water-filled case. The lower strain of the 50% water case is expected as the water acted to absorb impact energy, allowing deformation of the cylinder wall to decrease. The cases with pressurized annuli had a noticeably lower strain response as the internal pressure resisted deformation. The third largest strain value was seen in the 13.8 kPa (2 psi) case, with a value more than 25% less than that of the control. The sample that experienced the least deformation of the outer cylinder in the longitudinal direction was the 27.6 kPa (4 psi) case. This trend is interesting as it suggests an inverse relationship between peak force and peak strain. However, when the annulus condition is taken into account, another distinction can be made instead. It is clear that the internal pressure and density play a role in resisting deformation from a low-velocity impact force.

b. Front Hoop Strain "FY" Prior to Failure

The FY strain-time histories for each of the cases are similar in that each of the curves are sinusoidal in shape. The control and 50% water filled began as tensile strain, transitioned to compressive, and finally returned to compressive strain. The 13.8 kPa (2 psi) and 27.6 kPa (4 psi) exhibit a similar shape, two maxima and one minimum, and the strain values do not become compressive at any point. The oscillation of the strain direction is believed to be caused by the elastic rebound of the cylinder to its original shape after impact. However, within the pressurized annuli, the force imparted by the internal pressures do not allow for the material to enter compressive strain as the pressurized air would act to reduce the strain rate of the material. Similarly, in the graph of the 50% water-filled case there is clear reduction in the magnitude of the compressive strain as opposed to that in the control. This behavior is believed to be caused by the mass effect of the water, which acts to absorb the elastic energy of the cylindrical structure, reducing the energy available to cause strain within the cylinder walls.

In terms of the magnitude of tensile strain, the 27.6 kPa (4 psi) case exhibits the largest value of 6.19E-3, followed by the control, 50% water, and 13.8 kPa (2 psi) cases. The large tensile strain displayed by the 27.6 kPa (4 psi) case is likely caused by the increase of pressure in the annulus upon impact, which generated additional forces to displace the cylinder wall in the hoop direction to a greater degree than of any other case. In the case of the 13.8 kPa (2 psi) case, it is unclear as to why the tensile magnitude is significantly lower than that of the other cases. One possibility is that at 13.8 kPa (2 psi), the annuli conditions allow the cylinder walls to behave as a stiff elastic material. Furthermore, because the pressure within the annulus is relatively low, the deformation of the cylinder wall at the impact site is not sufficient to significantly increase the pressure load in the cylinder that would result in a drastic increase of tensile hoop stress.

c. Back Longitudinal and Hoop Strain "BX" and "BY" Prior to Failure

The magnitude of the strains recorded on the back of the cylinders were on average one order of magnitude lower than those recorded from the "FX" and "FY" strain gages. This was expected as deformation in this location occurred due to the force of impact propagating through the fluid medium. In the longitudinal directions, pressurized cases experienced a small gradual increase and subsequent decrease of compressive strains while the 50% water case exhibited oscillatory-like strain behavior and the control exhibited a negligible change. The periodic strain response of the 50% water case continued for a greater duration than the responses recorded in the other cases. The maximum strain values of the 50% water case were three times larger than those seen in 27.6 kPa (4 psi) case, the case with the next largest maximum value. This was expected, as after impact the water would slosh within the annulus, transferring energy from momentum into a force applied to the cylinder walls. The 27.6 kPa (4 psi) and 2 psi cases experienced similar compressive strains, with the 13.8 kPa (2 psi) case having slightly less peak strain, as expected.

Similar results are found when observing the hoop strain values. The control displayed a negligible strain response and the pressurized cases saw a slight increase in tensile strain. The 50% water case experienced decaying periodic hoop strain, again, nearly

three times larger than that of the 27.6 kPa (4 psi) case and lasted for a greater period of time.

4. Strain of Inner Cylinder Prior to Failure

The strain values recorded by the inner strain gages are illustrated in this section. The resultant strains depicted are largely the direct result of the FSI occurring within the annuli of the cylinders as the two separate structures were coupled via fluids. The force of impact would generate a pressure wave within the fluid media, which would then propagate through the fluid in the annulus, leading to measurable deformation occurring within the walls of the cylinder. The data collected show a significant decrease in magnitude of the measured strain as compared to that obtained from the outer cylinder strain gages. Generally, the annuli containing a fluid at the greatest density experienced the greatest magnitudes of strain measured at the inner cylinder. Figures 23 through 27 depict the average inner strain-time histories of each case in each direction and location.

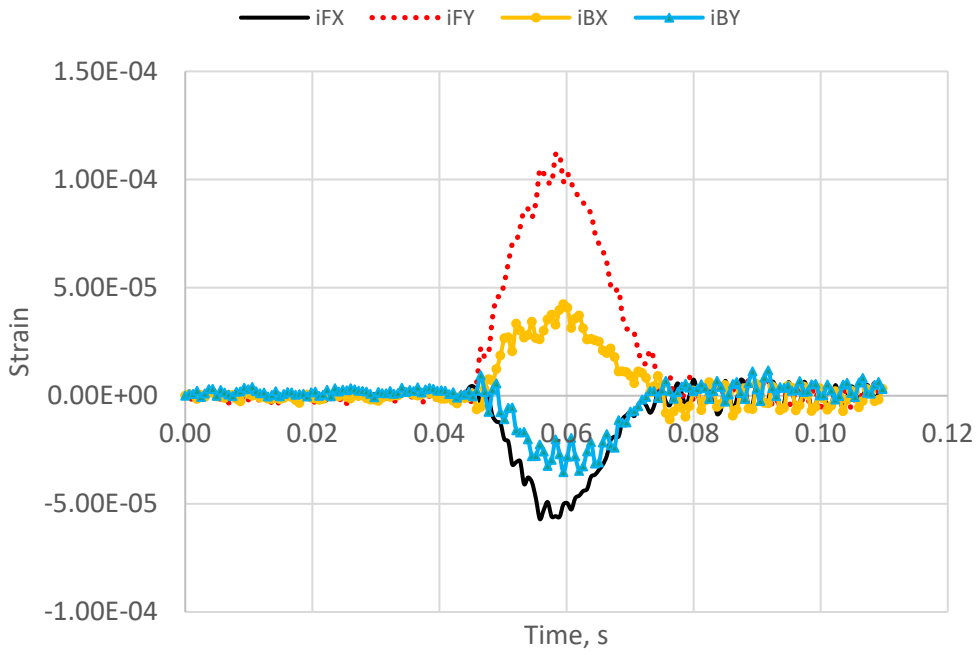

Figure 23. Inner Strain of Control

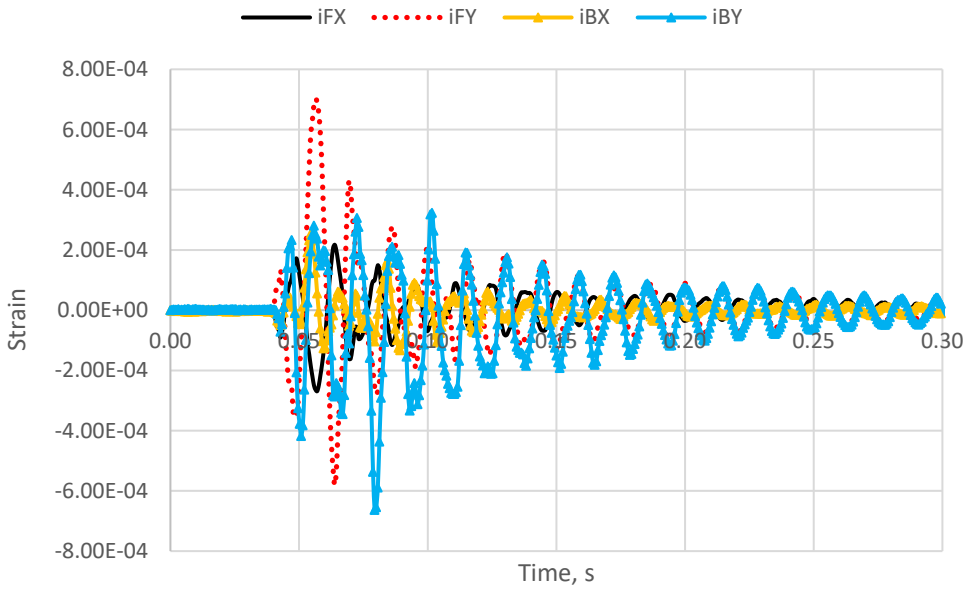

Figure 24. Inner Strain of 50% Water

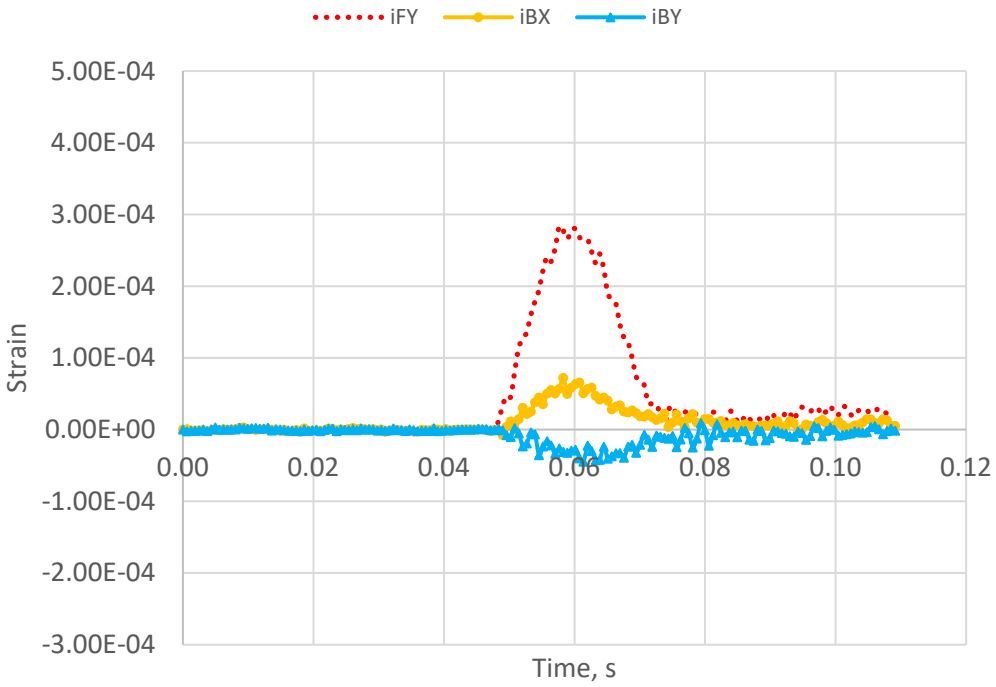

Figure 25. Inner Strain of 13.8 kPa

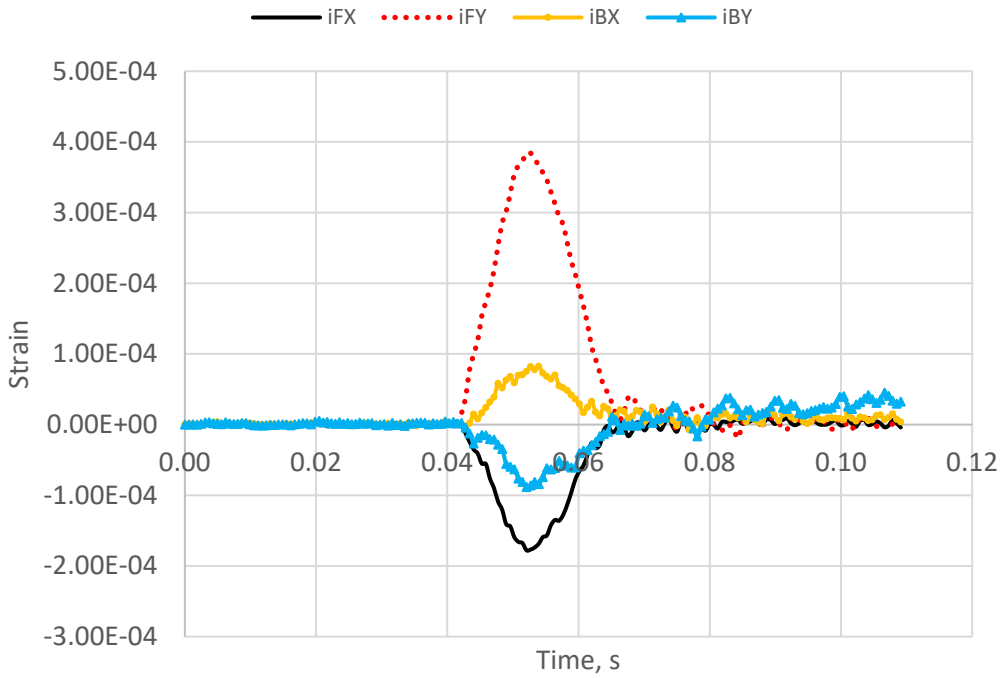

Figure 26. Inner Strain of 27.6 kPa

a. Inner Front Longitudinal Strain "iFX" Prior to Failure

Data was not recovered for the 13.8 kPa (2 psi) annulus case due to hardware issues. In all cases where strain was recorded, except for the 50% water case, the longitudinal strain in the inner cylinders were compressive and followed a half-sine curve that increased to a maximum and returned to zero. The 50% water filled case followed an exponentially decaying sine curve, with the greatest magnitude occurring as a compressive strain as shown in Figure 25. The case with the greatest magnitude strain value was the 50% water filled annulus, with a maximum compressive strain of -2.69E-4, one and a half times larger than the maximum value of the 27.6 kPa (4 psi) case and nearly five times as great as maximum value in the control. As expected, the magnitude of the strain is related to the properties of the fluid used to couple the structure.

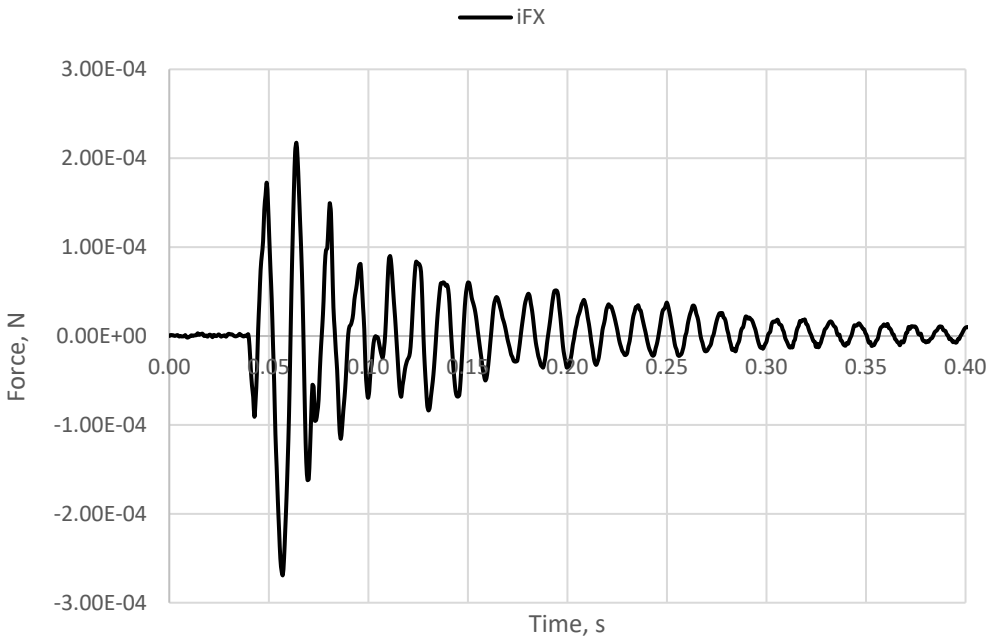

Figure 27. iFX Strain-Time History

b. Inner Front Hoop Strain "iFY" Prior to Failure

The results observed for the strain-time histories of the front inner hoop strain are similar in shape to those found for inner longitudinal strain. However, in each case, the magnitude of the hoop strain is significantly greater than that observed in the x-direction. The 50% water case exhibits the highest magnitude of hoop strain, with a maximum value of 6.91E-4. Much like the data recorded from the longitudinal strain gage, the data resembles an exponentially decaying sine curve, that oscillates between tensile and compressive hoop strain. As with before, the case with the second highest hoop strain was the 27.6 kPa (4 psi) case, at a value of 3.76E-4, followed by 13.8 kPa (2 psi) with 2.77E-4, and lastly the control, at 1.17E-4 peak strain. Interestingly, the shape of the curves produced by the inner strain-time histories are significantly different than those found on the outer cylinder. The data obtained from the outer cylinder strain gage depicts two distinct maximums and one distinct minimum, while those gathered from the inner strain gage show one maximum and subsequent relaxation of the material to zero. This is believed to

have occurred due to the pressure forces from impact acting externally on the inner cylinder through the fluid medium.

c. Inner Back Longitudinal and Hoop Strain "iBX" and "iBY" Prior to Failure

In all cases aside from the 50% water filled case, the longitudinal and hoop strains follow a half-sine shape, with the hoop direction being in compression, and the longitudinal direction under tension. The peak strains for each direction are at least one order of magnitude less than their counterparts located at the front side of the cylinder which demonstrates the loss of energy of the pressure wave within the fluid medium. Again, both longitudinal and hoop strains of the 50% water filled case resemble an exponentially decaying sine curve. Interestingly, the hoop strain found at the back of the inner cylinder is nearly equivalent to that found at the front of the inner cylinder, with a peak magnitude of -6.63E-4 that occurs approximately 0.22 seconds after the maximum hoop strain found at the front of the inner cylinder. The reason for the phenomenon is unclear, but may be related to a combination of the propagation of the pressure wave through the inner cylinder and the fluid medium.

5. Strain of Outer Cylinder at Failure

The strain occurring at the walls of the outer cylinder was measured while failure of the structure occurred. The resulting data is shown in Figures 28–33. Generally, the data show that in the case of an air-filled annuli, pressurized or not, the FSI within the annulus is similar to that found in the control case prior to failure. However, in a water filled annulus, the force of impact is more efficiently transferred through the fluid medium, resulting in increased deformation on the opposing wall.

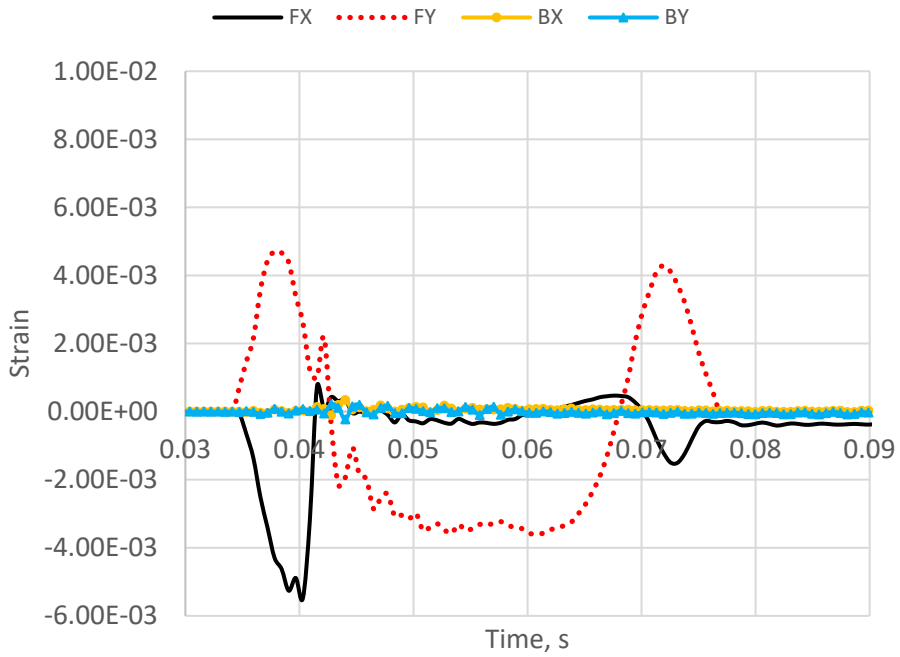

Figure 28. Outer Strain of Control at Failure

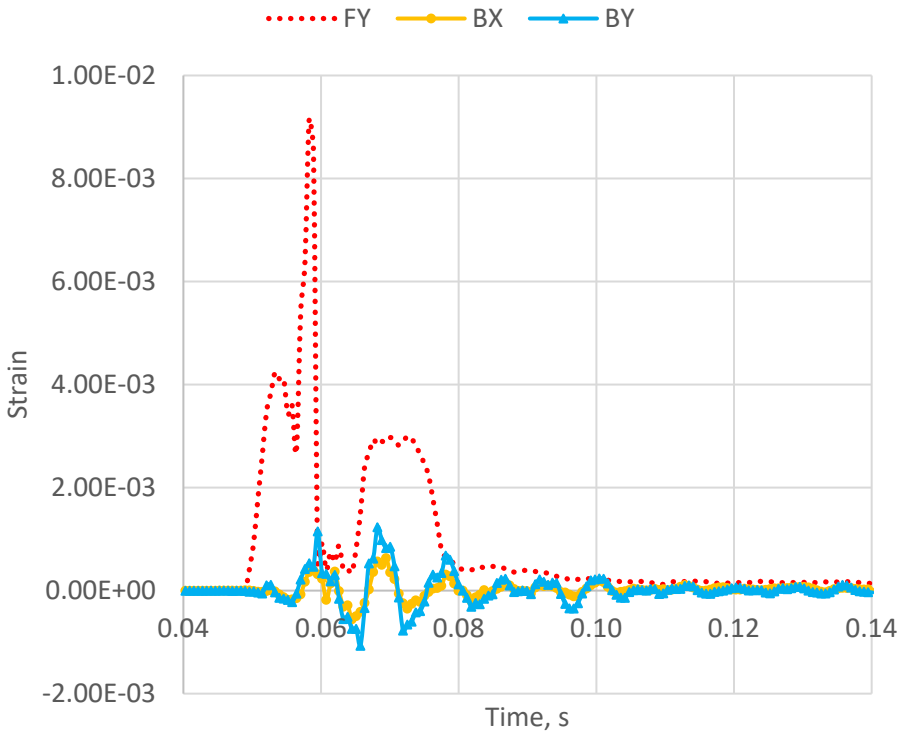

Figure 29. Outer Strain of 50% Water at Failure

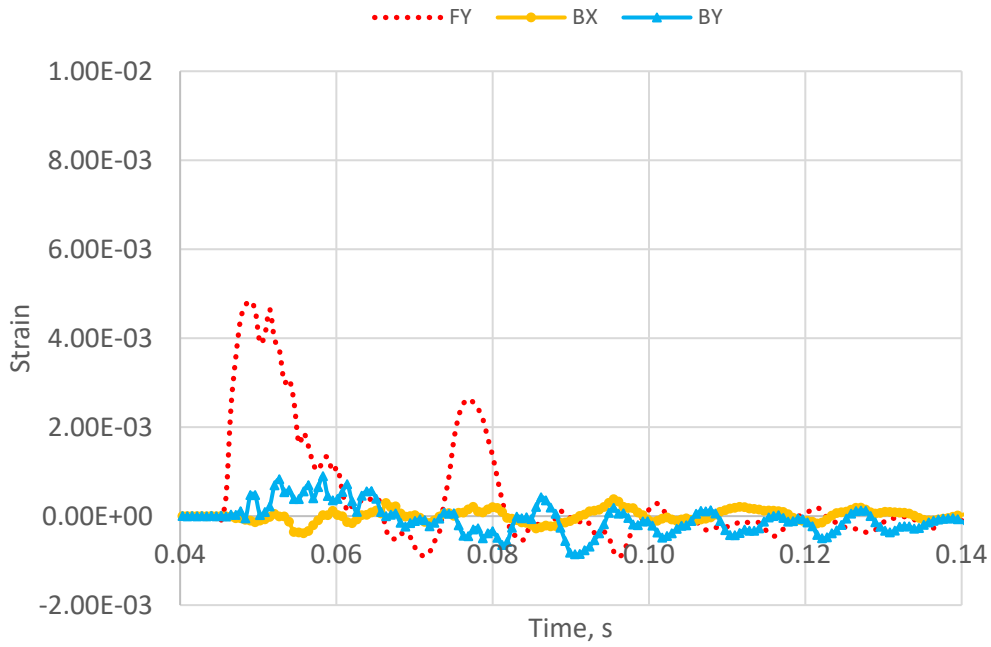

Figure 30. Outer Strain of 100% Water at Failure

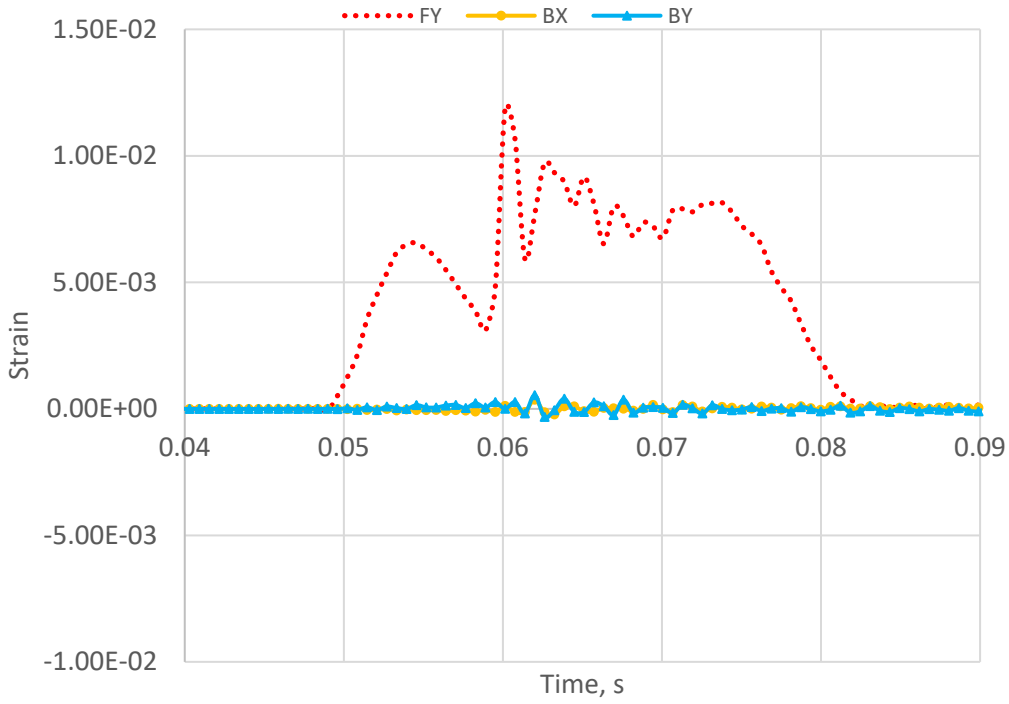

Figure 31. Outer Strain of 13.8 kPa at Failure

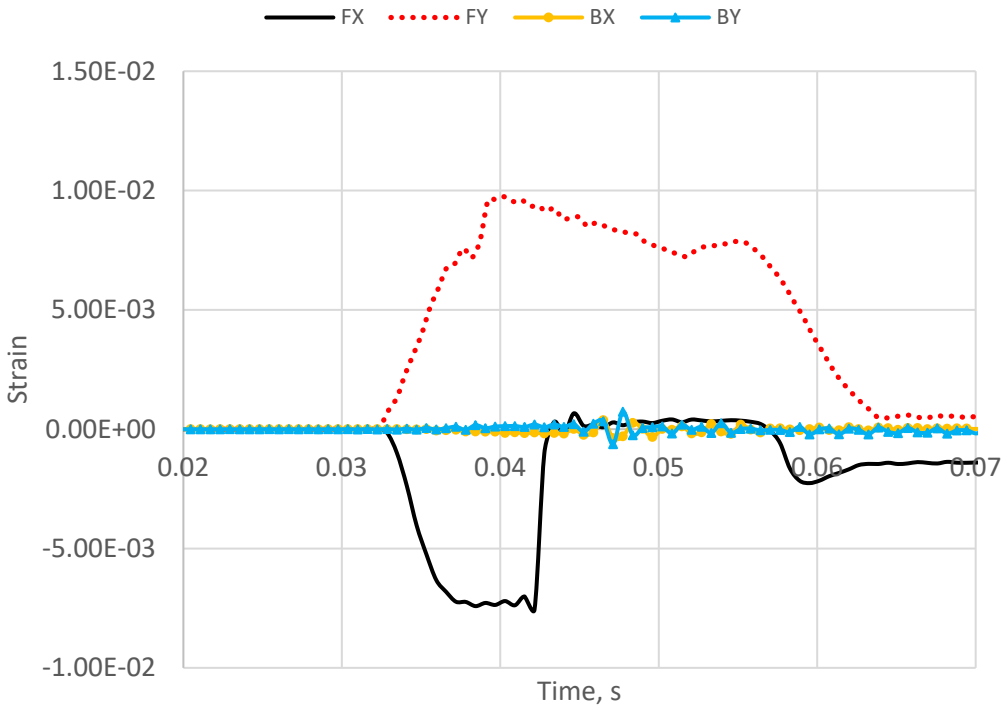

Figure 32. Outer Strain of 27.6 kPa at Failure

a. Outer Front Longitudinal Strain "FX" at Failure

Due to the failure crack propagating through the "FX" strain gage, strain data for this location was not captured for most cases during the final blow. However, in the cases where front longitudinal strain was collected, the control and 27.6 kPa (4 psi) cases, it is apparent that this was the controlling factor of failure as once impact occurs the longitudinal strain value immediately returns to zero. This is expected given that the failure occurred between the layers, perpendicular to the longitudinal axis. In the control case, failure occurred at a peak compressive strain of -5.48E-3 while failure occurred at a compressive strain of -7.56E-3 in the 27.6 kPa (4 psi) case. These values were unexpected, as before failure, the outer longitudinal strain values were consistently greater in the control case due to the lack of an internal pressure within the annulus. Additionally, in either case, after failure and return of the strain value to zero, there is a significant peak in compressive strain just before steady state is achieved. The mechanism behind this is unclear but may be caused by the release of residual stress from production after the failure has occurred.

b. Outer Front Hoop Strain "FY" at Failure

The strain responses of each case at failure are markedly different than that observed prior to failure, except for the control case. In the control case, the hoop strain behaves sinusoidally with two tensile maximums and one compressive minimum in both failure and prior to failure conditions. In the 50% water case, two tensile maximums can be distinctly observed, however, the hoop strain does not enter into a compressive state as seen prior to failure. The hoop strain seen in the 100% water filled case behaves like an exponentially decaying sine curve that oscillates to a greater tensile strain than compressive strain. This behavior is expected given the incompressible nature of the water, allowing the pressure wave to propagate throughout the annulus until the energy is dissipated as heat and deformation of the cylinder walls. The hoop strain found in the 13.8 kPa (2 psi) case is purely compressive, just like as seen in the hoop strain associated with the before failure condition. However, there strain-time history shows several local maximums and minimums, with one large peak occurring roughly midway through the excitation of the structure, which is not seen before failure condition. In the 27.6 kPa (4 psi) case, the strain-time history shows a tensile strain that is trapezoidal in shape. This is significantly different than the before failure condition, where the strain behavior is sinusoidal, with two local maximums and one local minimum. In either case, the strain does not oscillate due to the release of internal pressure once failure occurs.

When comparing the magnitude of the front hoop strain between the failure and non-failure condition, there is a significant difference within all cases. In all cases aside from the control, the strain in the hoop direction was greater during failure. This was most apparent is in the 13.8 kPa (2 psi) case, where the strain is nearly three times greater during failure as opposed to before. The 50% water case exhibits the second largest difference, followed by the 27.6 kPa (4 psi) and finally the control cases. Interestingly, the control case is the only case with available data that has a greater peak hoop strain before failure than during failure. The mechanism as to why this occurred has not been identified, but may be the result of impact fatigue. The peak strain generally increased with the number of blows, indicating larger deformations of the cylinder. This, in combination of the lack of internal pressure, likely significantly decreased the yield strain just before failure occurred.

c. Outer Back Longitudinal and Hoop Strain "BX" "BY" at Failure

In the air-filled annuli, control, 13.8 kPa (2 psi), and 27.6 kPa (4 psi), the longitudinal and hoop strains recorded at the back of the cylinder are similar to those found in the control case before failure. There was no significant strain response to impact. Instead, in the case of the pressurized annuli, any response can be attributed to the return of the cylinder to its original position prior to pressurization as the internal pressure is released from the point of failure.

The longitudinal and hoops strains in the 50% water case exhibited similar behavior to that found in the before failure condition. Both directions of strain are represented as a decaying sine wave, however, in the failure case, the magnitude of the strain is significantly greater. The peak strains in both directions are nearly four times greater than that of the before failure condition. This aligns with the fact that after failure, greater strains were observed at the front of the cylinder. This larger displacement of the cylinder walls displaced a greater mass of water, allowing for a larger pressure wave that propagated through the fluid and displaced the back cylinder wall to a greater extent. In the case of 100% water, similar behavior is observed, although the peak strains are of lower magnitude. As with the strain measured at other locations, this is due to the mass of the water. While the strain magnitudes are lower, the duration of the response is much longer as the incompressible nature of the water filled annulus allows for the impact energy to be transmitted through the fluid more efficiently.

6. Strain of Inner Cylinder at Failure

Figures 33–38 show the strain data of the inner cylinders at failure. The data obtained for the control and 13.8 kPa (2 psi) cases include significant interference that was not a result of the FSI within the cylinder, but rather that of vibrations caused by the rapid failure of the cylinder wall. Thus, those datasets will not be analyzed in this section. Furthermore, as it is impossible to discern between strain caused from impact or strain caused from depressurization of the annulus, the 27.6 kPa (4 psi) case is not compared with previous data as it is likely the FSI of the inner cylinder was negligible, as seen with previous results. The results that could be compared varied and thus definitive conclusions

could not be made. However, the 100% water case experienced the greatest magnitude of strain at the inner cylinder with peak magnitudes on average one order of magnitude greater than that found in the same location within the 50% water case.

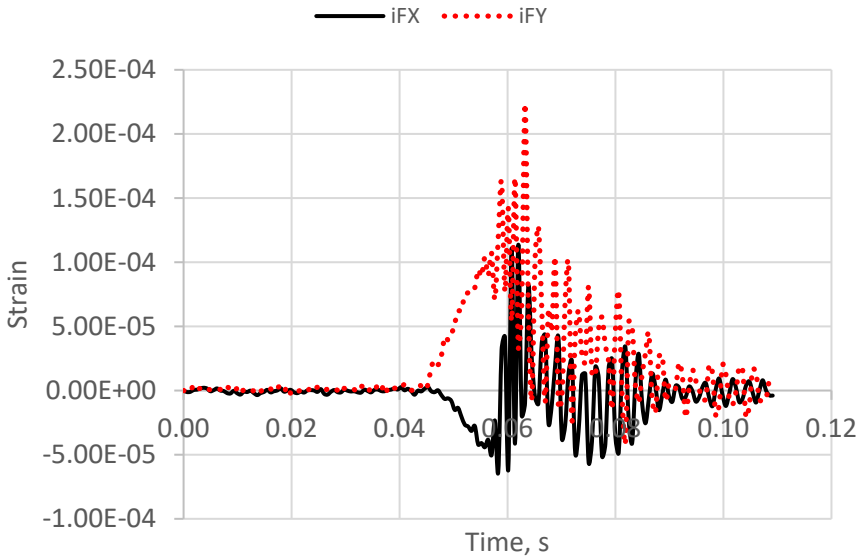

Figure 33. Inner Front Strain of Control at Failure

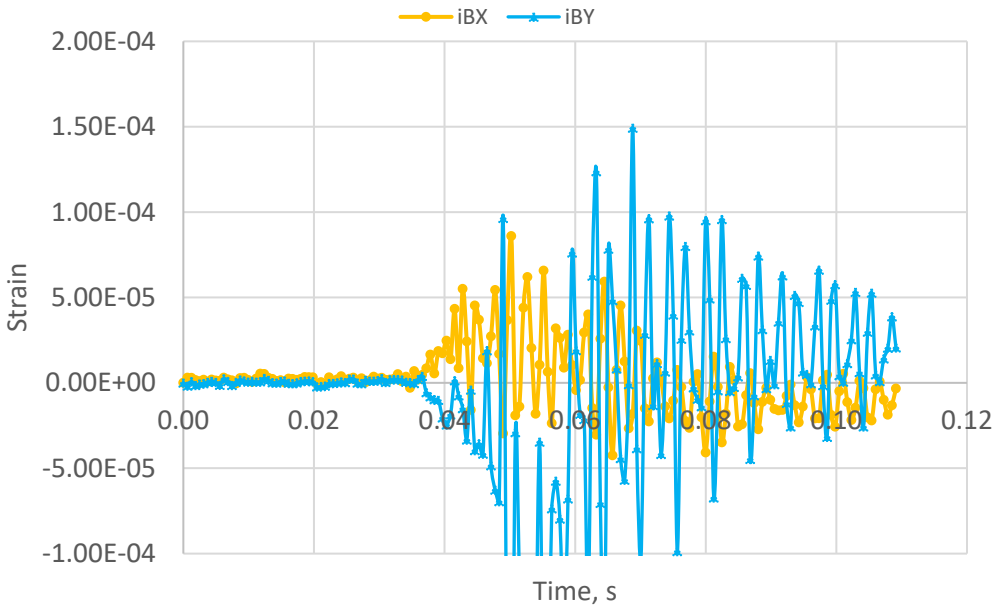

Figure 34. Inner Back Strain of Control at Failure

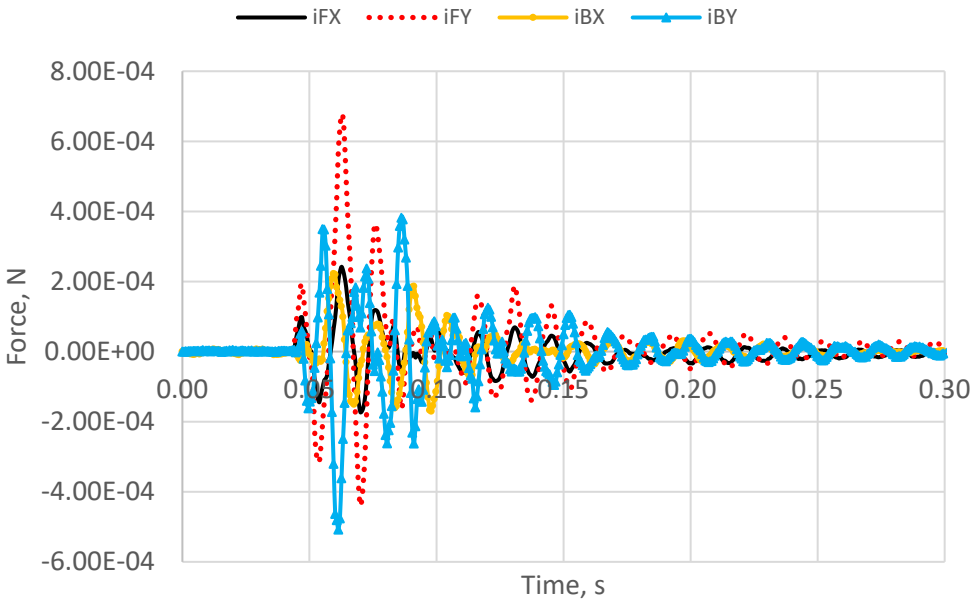

Figure 35. Inner Strain of 50% Water at Failure

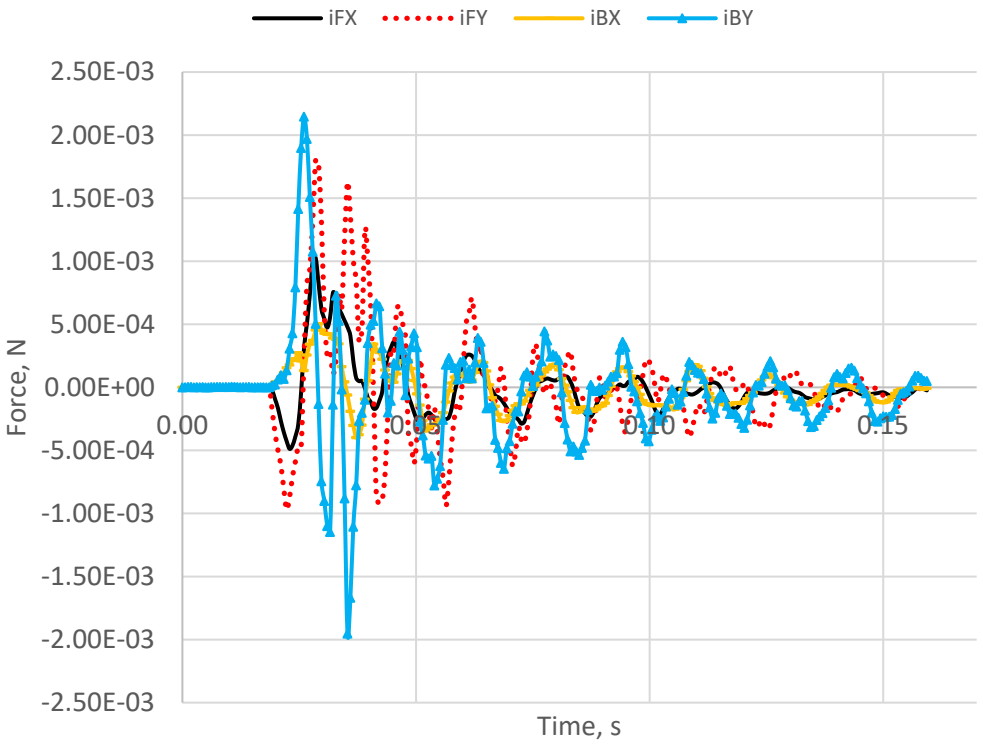

Figure 36. Inner Strain of 100% Water at Failure

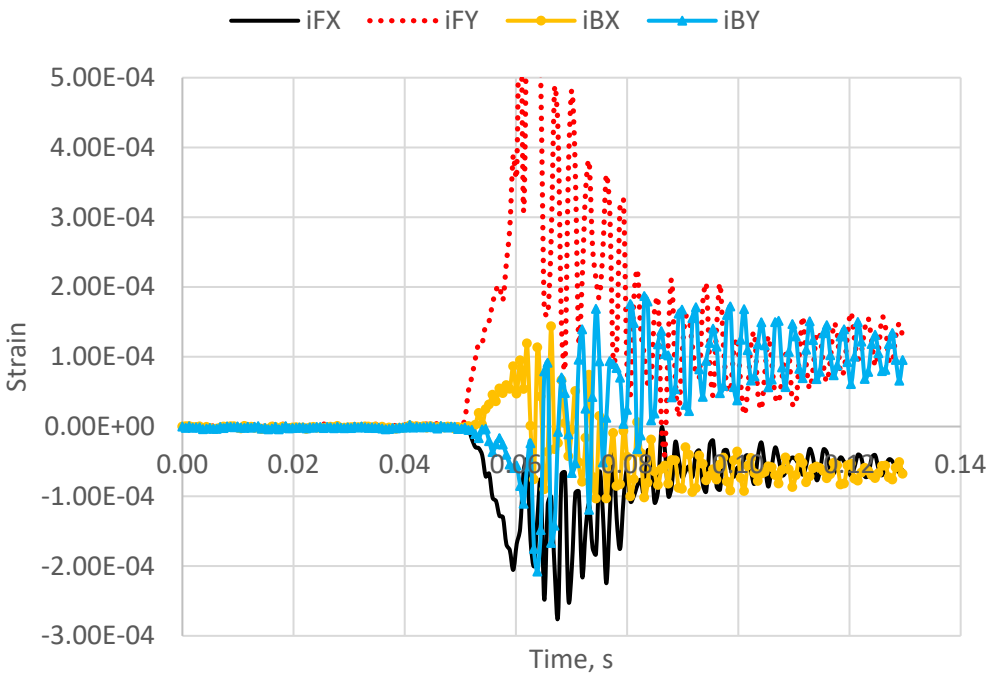

Figure 37. Inner Strain of 13.8 kPa at Failure

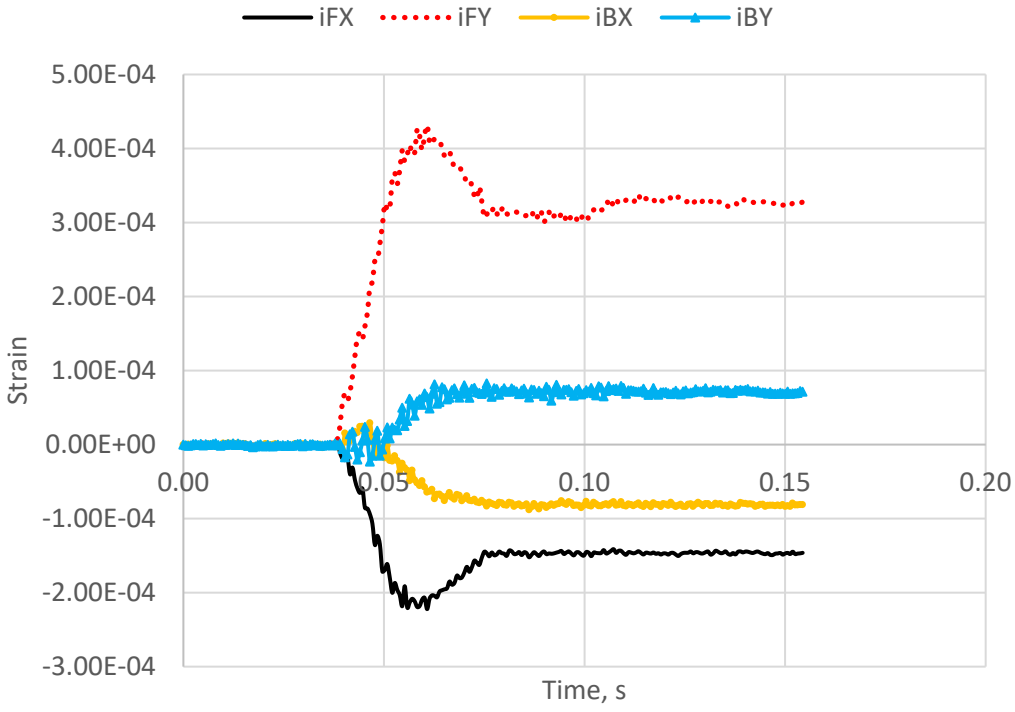

Figure 38. Inner Strain of 27.6 kPa at Failure

a. Inner Front Longitudinal Strain "iFX" at Failure

For the cases that can be compared to the non-failure condition, the 50% water case, the results vary. The longitudinal strain maintains the same shape as before, an exponentially decaying sine curve; however, the magnitude is less than that found in the non-failure condition by roughly 8% for both the tensile and compressive maximums. This disputes the trend observed in previous data, where the maximum inner strain generally increased at locations away from the impact point during failure. The reasoning for this dispute is not clear and may be the result of experimental error. The 100% water inner longitudinal strain behaved similarly to that of the 50% water case. However, in this case, the peak strain magnitude was one order of magnitude larger and oscillated at a higher frequency than that found in the 50% water case due to the increased mass and average density within the annulus.

The magnitudes varied greatly throughout the different annulus cases, with the greatest, at 1.03E-3 belonging to the 100% water case, followed by the 50% case at 2.42E-4. While the maximum strain values could not be analyzed for the control and 13.8 kPa (2 psi) cases, given the previous set of data, it is reasonable to conclude that the strains in the longitudinal direction were negligible due to the lack of FSI occurring.

b. Inner Front Hoop Strain "iFY" at Failure

Again, the strain data received for the inner hoop direction in the control and 13.8 kPa (2 psi) cases are not sufficient to draw conclusions from. Similarly, the data obtained from the 27.6 kPa (4 psi) case are do not allow any for any conclusive results due to the relaxation of the cylinder walls. Furthermore, the shapes of both 50% and 100% water cases are similar to previously found as both are exponentially decaying sine waves with the greatest magnitude strain occurring in the tensile direction. When comparing the 50% water's hoop strain with that before failure, the result is similar to that found in the longitudinal direction. In the failure condition, the peak tensile strain is roughly 4% less than that found in the non-failure condition. Again, this discrepancy is like the result of experimental error of the failure blow as previous results overwhelmingly suggest

otherwise. Within the 100% water case, the peak strain is roughly 2.5 times that of the 50% case as expected.

c. Inner Back Longitudinal and Hoop Strain "iBX" and "iBY"

Again, the cases with a liquid filled annulus follow an exponentially decaying sine curve. For the 50% case, the hoop strain varies significantly from failure to the non-failure condition. While both curves exhibit a maximum peak strain in compression, once again, the strain values are larger in the non-failure case by approximately 26%. As for the inner back longitude strain, the peak strain is tensile and the results align with those found previously. The peak strain at this location at failure is nearly twice as large as that found in the non-failure condition. In the 100% case, the results align with those in the 50% water case, just at a magnitude nearly twice that of the 50% case for each direction. The inner back hoop strain is significantly larger than the inner back longitudinal strain by a factor of 4 and are both in tension; this is expected as the pressure wave generated by the impact acts perpendicular to all surfaces.

THIS PAGE INTENTIONALLY LEFT BLANK

IV. CONCLUSIONS AND RECOMMENDATIONS

This thesis sought to analyze the force and strain response and FSI of two fluid-coupled concentric cylinders when subjected repeatedly to a low velocity impact load until failure through experimentation. The cylinders used were manufactured using fused filament fabrication (FFF), a 3D printing process, and the material selected was PLA. Strain gages were attached to the cylinder to measure longitudinal and hoop strain at the front and back of the inner and outer cylinders and a force gage was attached to an impactor at the end of a pendulum. The gages were used to collect data on the strain and force response of the 3D printed cylinders with various conditions in which they were coupled. The experimental design includes the testing of three primary annulus conditions: air filled, water filled, and pneumatically pressurized. Within the primary cases, four subcases were tested: 50% water filled, 100% water filled, pressurized to 13.8 kPa (2 psi), and pressurized to 27.6 kPa (4 psi). Experimentation involved dropping a pendulum from a 45° angle and allowing a semi-spherical steel impactor to impact the center of the cylindrical structure. This was repeated until failure, where the number of blows until failure, and strain and force data were recorded. The strain and force data were then analyzed to determine how the various annuli conditions affect the strain and force response of the structure prior to and at failure.

Before failure, the force-time history resembled a half-sine curve and varied as a function of annulus condition. Specifically, the annulus condition with the greatest peak force was the 27.6 kPa (4 psi) case, then 13.8 kPa (2 psi) case, followed by the control, and finally the 50% water case. Once failure occurred, the force-time history showed that once the peak force was reached, the force steeply decreased and returned to zero. The data of the force-time histories aligned with the data concerning the number of blows until failure as it is expected that the case subjected to the greatest force would, within error, fail sooner when the same drop angle is used.

Through analysis of the strain time histories, it is evident that the strain response is a function of annulus condition. Before failure, the stains measured at the point of impact were lower in the water filled and pressurized annulus cases as compared to the control,

with the 13.8 kPa (2 psi) case exhibiting the greatest resistance to deformation. However, at locations other than the impact point, inverse is observed as the water filled annulus exhibited the greatest magnitude of strain of the inner cylinder and backside of the front cylinder, followed by the pressurized cases, and lastly the control. This suggests a more efficient coupling of the structures in fluids with a greater density.

At failure, the strain response at the impact point of the cylinder significantly increased in magnitude as compared with the non-failure condition in each annulus case. The strains observed at the inside cylinder and at the opposing wall of the air-filled cases, regardless of pressurization, exhibited a negligible strain response during failure, suggesting little to no FSI at failure. The water filled cases continued experiencing a high degree of FSI, with the 100% water case exhibiting the greatest deformation of the cylinder walls in both the inner and outer cylinders. The strain response of the outer and inner back walls increased significantly at failure in the 50% water case, suggesting that at failure, the energy imparted into the failure is greater than before failure.

While the understanding of the FSI occurring before and during failure of this geometry is better understood due to this research, further analysis would greatly benefit the depth of understanding. In the future, it is recommended that future researchers utilize computer modeling software to simulate the experimental setup and annulus conditions used within this paper. It is also recommended that a finite elemental analysis be completed of the structure at various annulus condition. Furthermore, the experimental testing of other annulus conditions should be conducted. Through this research, it was validated that annuli conditions affect the force and strain response of a concentric cylinder structure before and during failure. By varying the annulus conditions further, such as by pressurizing with water, or at various percentages of water, the degree at which the structures are coupled through FSI would change.

LIST OF REFERENCES

[1] Kaneko, S., Nakamura, T., Inada, F., Kato, M., Ishihara, K., Nishihara, T., and Langthjem, M. A., eds., 2014, "Chapter 1 – Introduction," *Flow-Induced Vibrations* (2nd ed.), Academic Press, Oxford, pp. 1–28.

[2] Eder, B., "Critical Wind Mitigation for Mega-Tall Structures," *Structure Magazine,* July 2016.

[3] Vathi, M., Karamanos, S. A., Kapogiannis, I. A., and Spiliopoulos, K. V., 2017, "Performance Criteria for Liquid Storage Tanks and Piping Systems Subjected to Seismic Loading," *J. Press. Vessel Technol*., 139(051801).

[4] Shams, A., Lopresto, V., and Porfiri, M., 2017, "Modeling Fluid-Structure Interactions during Impact Loading of Water-Backed Panels," *Compos. Struct*., 171, pp. 576–590.

[5] Moscoloni, C., Kwon, Y. W., Didoszak, J. M., and Mattiazzo, G., 2019, "Dynamic Response of Tube Containing Water Subjected to Impact Loading," *Multiscale Multidiscip. Model. Exp. Des*., 2(4), pp. 281–290.

[6] Kwon, Y., and Bowling, J., 2018, "Dynamic Responses of Composite Structures Coupled through Fluid Medium," Multiscale Multidiscip. Model. Exp. Des., 1.

[7] Kwon, Y. W., 2009, "Study of Fluid Effects on Dynamics of Composite Structures," *Volume 4: Fluid-Structure Interaction*, ASMEDC, Prague, Czech Republic, pp. 647–654.

[8] Alaei, D., Kwon, Y. W., and Ramezani, A., 2019, "Fluid-Structure Interaction on Concentric Composite Cylinders Containing Fluids in the Annulus," *Multiscale Multidiscip. Model. Exp. Des*., 2(3), pp. 185–197.

[9] "UltiMaker S5: Reliability at Scale," UltiMaker, accessed April 11, 2023, https://ultimaker.com/3d-printers/ultimaker-s5.

[10] Pandzic, A., and Hodzic, D., 2021, "Mechanical Properties Comparison of PLA, Tough PLA and PC 3D Printed Materials with Infill Structure – Influence of Infill Pattern on Tensile Mechanical Properties," *IOP Conf. Ser. Mater. Sci. Eng*., 1208(1), p. 012019.

[11] Nachazel, T., 2020, *What Is a Strain Gauge and How Does It Work*?, Mich. Sci. Corp., MI.

[12] Perez, D. B., Celik, E., and Karkkainen, R. L., 2021, "Investigation of Interlayer Interface Strength and Print Morphology Effects in Fused Deposition Modeling 3D-Printed PLA," *3D Print. Addit. Manuf.*, 8(1), pp. 23–32.

INITIAL DISTRIBUTION LIST

1. Defense Technical Information Center
   Ft. Belvoir, Virginia

2. Dudley Knox Library
   Naval Postgraduate School
   Monterey, California